nature neuroscience

ARTICLES

https://doi.org/10.1038/s41593-018-0127-z

Tbr1 instructs laminar patterning of retinal ganglion cell dendrites

Jinyue Liu[1,2,3], Jasmine D. S. Reggiani[1,2], Mallory A. Laboulaye[1,2], Shristi Pandey[1,2], Bin Chen[4], John L. R. Rubenstein[5], Arjun Krishnaswamy[1,2,6] and Joshua R. Sanes[1,2*]

Visual information is delivered to the brain by >40 types of retinal ganglion cells (RGCs). Diversity in this representation arises within the inner plexiform layer (IPL), where dendrites of each RGC type are restricted to specific sublaminae, limiting the interneuronal types that can innervate them. How such dendritic restriction arises is unclear. We show that the transcription factor Tbr1 is expressed by four mouse RGC types with dendrites in the outer IPL and is required for their laminar specification. Loss of Tbr1 results in elaboration of dendrites within the inner IPL, while misexpression in other cells retargets their neurites to the outer IPL. Two transmembrane molecules, Sorcs3 and Cdh8, act as effectors of the Tbr1-controlled lamination program. However, they are expressed in just one Tbr1$^+$ RGC type, supporting a model in which a single transcription factor implements similar laminar choices in distinct cell types by recruiting partially non-overlapping effectors.

Many regions of the nervous system are arranged into parallel laminae. Neurons that synapse in these areas often confine their axons and dendrites to one or a few of these laminae, restricting their choice of synaptic partners. Laminar specificity is so widespread that it appears to be a major determinant of specific connectivity[1,2].

A particularly striking instance of laminar specificity occurs in the vertebrate retina. In mouse, dendrites of >40 retinal ganglion cell (RGC) types arborize in a synaptic layer called the inner plexiform layer (IPL), with dendrites of each type restricted to one or a few of at least 10 sublaminae. There, they receive synapses from ≥ 70 types of interneurons (amacrine and bipolar cells) whose processes also arborize in specific IPL sublaminae. This stereotyped, stratified arrangement restricts the interneuronal types that can innervate each RGC type, thereby tuning the latter to specific visual features[3]. The best studied example is an ON–OFF bipartite division of the IPL; RGCs that project dendrites to the outer half of the IPL receive inputs from bipolar cells that are excited by decrements in illumination levels (OFF responses), whereas those that project to the inner half receive inputs from bipolar cells that are excited by increments (ON responses). Consequently these two groups of RGCs are termed OFF- and ON-types, respectively[4]. Further dendritic restrictions within these zones are associated with additional distinctions in RGC response type[5].

Multiple cell-surface molecules have been shown to mediate intercellular interactions in the IPL, leading in some cases to targeting of neurites to specific sublaminae. They include members of the immunoglobulin[6–9] and cadherin superfamilies[10], semaphorins, and plexins[11,12]. In contrast, little is known about how the expression of these cell-surface molecules is coordinated to specify laminar targeting of dendrites. Here we identify the transcription factor T-box brain 1 (Tbr1) as one such regulator. We show that Tbr1 is selectively expressed by four RGC types, all of which bear dendrites that arborize in the outer third of the IPL. Intrigued by this commonality, we used loss- and gain-of-function approaches to ask whether Tbr1 is involved in dendritic targeting. We found that it is required for laminar patterning of Tbr1-expressing RGCs and can retarget dendrites of other neuronal types to the outer IPL when ectopically expressed. We then identified two cell-surface molecules, cadherin 8 (Cdh8) and sortilin-related VPS10 domain containing receptor 3 (Sorcs3), as downstream effectors of Tbr1; both restrict dendrites of one Tbr1-expressing RGC type, J-RGC[13], to the outer IPL. Strikingly, however, Cdh8 and Sorcs3 are not expressed by the other three Tbr1-expressing RGC types. These results suggest that Tbr1 recruits at least partially distinct sets of downstream effectors to specify laminar identity in the different RGC types that express it.

Results

Four RGC types express Tbr1. To identify markers and potential regulators of specific RGC types, we analyzed the expression of transcription factors in mouse retina[14]. Tbr1 was expressed by ~15% of RGCs but by no other retinal cells (Fig. 1a,b). To date, no single RGC type in mouse has been found to account for more than 10% of total RGCs[3]. We therefore suspected that Tbr1 labeled multiple RGC types.

To assess the number and identity of what we will call 'Tbr1-RGC' types, we co-stained retinas with Tbr1 plus molecular markers expressed by RGC subsets, including other transcription factors. Tbr1-RGCs did not appreciably express FoxP2, which marks four F-RGC types[14]; Satb1, which is enriched in four ON–OFF direction-selective RGC (ooDSGC) types[9,15]; or Tbr2, which marks five intrinsically photosensitive RGC types[16,17] (Supplementary Fig. 1a). Instead, we found that subsets of Tbr1-RGCs expressed robust levels of Brn3b, Brn3c, osteopontin (Opn; gene symbol *Spp1*), or calretinin (Fig. 1c).

To determine whether these marker pairs labeled distinct RGC types, we made use of a feature of retinal neurons called mosaic spacing: neurons of the same type are less likely to be near neighbors than would be expected by chance, whereas they are randomly distributed with respect to cells of other types[18,19]. When viewed in

[1]Department of Molecular and Cellular Biology, Harvard University, Cambridge, MA, USA. [2]Center for Brain Science, Harvard University, Cambridge, MA, USA. [3]Program in Neuroscience, Harvard Medical School, Boston, MA, USA. [4]Department of Molecular, Cell and Developmental Biology, University of California at Santa Cruz, Santa Cruz, CA, USA. [5]Department of Psychiatry, University of California at San Francisco, San Francisco, CA, USA. [6]Present address: Department of Physiology, McGill University, Montreal, QC, Canada. *e-mail: sanesj@mcb.harvard.edu

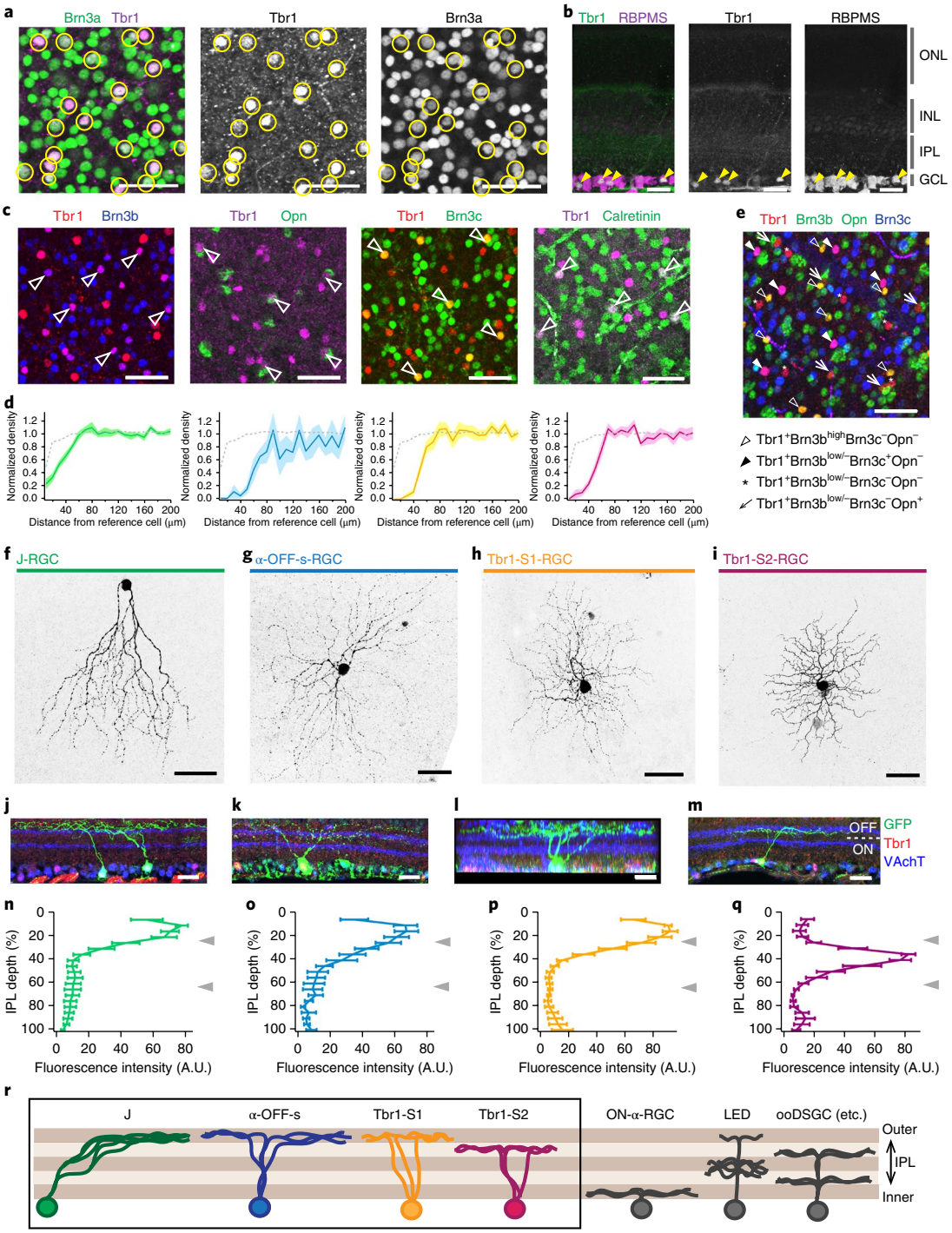

Fig. 1 | Expression of Tbr1 in four types of OFF-laminating RGCs. a, P21 retinal whole-mount stained with antibodies to Tbr1 and Brn3a, an RGC marker. A subset of RGCs is Tbr1$^+$. Yellow circles mark Tbr1$^+$ soma. Scale, 50 μm. **b**, Cross-section of P12 retinas showing Tbr1 expression exclusively in RGCs, marked with RBPMS. ONL, outer nuclear layer; INL, inner nuclear layer; GCL, ganglion cell layer. Arrowheads mark Tbr1$^+$Rbpms$^+$ RGCs. Scale, 25 μm. **c**, Whole-mounts showing that subsets of Tbr1-RGCs express Brn3b, Opn, Brn3c, or calretinin (arrowheads). Brn3b and Brn3c are nuclear, Opn is perinuclear, and calretinin is cytosolic. Scale, 50 μm. **d**, Density recovery profiles (DRP) for soma co-expressing each marker pair in **c**. Solid line represents mean and shaded bounds indicate standard error. Dotted gray line indicates normalized density of a heterogeneous population consisting of multiple cell types (in this case, the entire Tbr1$^+$ population; $n = 4$ fields per retina, 3 retinas per marker pair, each retina from a different animal). **e**, Whole-mount of retina stained with a combination of Tbr1, Brn3b, Opn, and Brn3c, showing four non-overlapping populations of Tbr1-RGCs. Each population is marked by an open triangle, closed triangle, asterisk, or arrow as indicated below the image. Scale, 50 μm. **f**–**i**, Tbr1-RGCs labeled in whole-mounts showing dendritic morphologies of each type. Scale, 50 μm. **j**–**m**, Cross-sections (**j**,**k**,**m**) or rotated view (**l**) of each Tbr1-RGC type from *JAM-B-CreER;Thy1-STOP-YFP* (**j**), W7 (**k**), YFP-H (**l**) and *Cdh4-CreER;Thy1-STOP-YFP* (**m**) mice. Scale bar, 25 μm. **n**–**q**, Quantification of the dendritic stratification for each Tbr1-RGC type ($n = 7$ J-RGCs, 8 α-OFF-s RGCs, 6 Tbr1-S1 RGCs, and 6 Tbr1-S2 RGCs, from 3 animals each). Line plot and brackets indicate average and standard error. Grey arrowheads mark positions of S2 and S4 as indicated by VAchT immunostaining. **r**, Schematic summarizing dendritic stratification of Tbr1-RGCs in comparison to other RGC types. All Tbr1-RGCs laminate dendrites within the outer third of the IPL. Each experiment in **a**–**c**,**e** and **f**–**m** was repeated independently in three animals with similar results.

whole mounts, somata co-labeled by each marker pair formed a uniformly spaced mosaic, as judged by the density recovery profile statistic[20], and were therefore likely to represent a single type (Fig. 1c,d). Exclusion zone size and soma density varied with each marker pair, indicating that they defined four different RGC types (Supplementary Fig. 1b). They populated the entire retina, making up 1.8% (Tbr1$^+$Opn$^+$) to 6.5% (Tbr1$^+$Brn3b$^+$) of RGCs and totaling ~15% of all RGCs (Supplementary Fig. 1c–g). Co-immunostaining for Tbr1 with combinations of Brn3b, Brn3c, Opn, and calretinin confirmed that the four types are non-overlapping (Fig. 1e and Supplementary Fig. 1h). Together, these four RGC types account for most if not all Tbr1$^+$ retinal cells.

Tbr1-RGCs laminate in the outer strata of the IPL. To assess the morphology of Tbr1-RGCs, we screened transgenic lines in which RGC subsets are labeled with a fluorescent protein. No labeled RGCs were Tbr1$^+$ in lines that selectively marked ooDSGCs[21] or W3-RGCs[22] (Supplementary Fig. 1m,n). However, all J-RGCs labeled in *JAM-B-CreER;Thy1-STOP-YFP*[13] mice were Tbr1$^+$Brn3b$^+$ (Fig. 1f,j and Supplementary Fig. 1i), and all alpha-OFF-sustained RGCs (α-OFF-s-RGCs) labeled in TYW7[22–24] mice were Tbr1$^+$Opn$^+$ (Fig. 1g,k and Supplementary Fig. 1j), identifying two previously characterized types as Tbr1$^+$.

The other two Tbr1-RGC types appeared novel. We therefore sought their identities in mouse lines that label multiple RGC types sparsely[14,25]. Tbr1 + Brn3c marked RGCs with radial dendrites that laminated within sublamina (S) 1 of the IPL; we follow the convention of dividing the IPL into five equal strata, S1–S5 (Fig. 1h,l and Supplementary Fig. 1k). Tbr1 + calretinin marked another RGC type; its dendrites abutted those of OFF starburst amacrine cells in S2 and bore spine-like protrusions that arose perpendicularly from their parent branches (Fig. 1i,m and Supplementary Fig. 1l). We will refer to these two types as Tbr1-S1-RGCs and Tbr1-S2-RGCs, respectively.

The ability to label Tbr1-RGCs allowed us to assess their topographic distributions, dendritic field areas, and coverage factors. α-OFF-s-RGCs displayed a temporal-high–nasal-low gradient as previously described[26]; J-RGCs displayed a dorsal-low–ventral-high gradient; and the two novel RGC types displayed shallow center-to-periphery gradients (Supplementary Fig. 1c–f). J-RGCs had the highest coverage factor, while α-OFF-s-RGCs had the largest dendritic area (Supplementary Fig. 1o,p). Notably, however, dendrites of all four Tbr1-RGC types were restricted to the outer third of the IPL, with three restricted to the outermost sublamina (S1), and the fourth type to S2 (Fig. 1j–r).

Tbr1 is required for laminar specification of RGC dendrites. Before assessing the role of Tbr1 in the retina, we determined its expression pattern through development. Tbr1 immunoreactivity was undetectable at embryonic day (E) 13.5, when RGC production is reaching its peak[27]. Over the next few days, Tbr1 appeared in postmitotic cells; by E17.5, it was confined to a subset of RGCs that were already non-overlapping with FoxP2$^+$ and Tbr2$^+$ cells (Supplementary Fig. 2a–c). This suggests that Tbr1 could regulate aspects of RGC development, including dendritic morphogenesis, which begins around birth (postnatal day (P) 0)[28].

Because constitutive Tbr1 mutant mice die perinatally[29], we generated conditional Tbr1 mutants to test this possibility (Supplementary Fig. 3a). We first deleted Tbr1 throughout the retina using a line that expresses Cre in embryonic retinal progenitors (*Tbr1^{loxP};Six3^{Cre}*, henceforth *Tbr1^{ret}*). Pan-retinal deletion of *Tbr1* had no detectable effect on retinal architecture or RGC numbers (Supplementary Fig. 3b).

We then deleted Tbr1 selectively from J-RGCs using the JAM-B-CreER line (*Tbr1^{loxP};JAM-B-CreER;Thy1-stop-YFP*, henceforth *Tbr1^{J}*; tamoxifen delivered at E14.5 or P0) and verified by immunostaining that ~95% of YFP-labeled J-RGCs lost Tbr1. Notably, ~65% of these Tbr1-deficient J-RGCs developed ectopic dendrites. Although they retained dendritic branches in S1, they also extended dendrites into S4, within the inner (ON) region of the IPL ($P = 1.2 \times 10^{-6}$, Cochran–Armitage test; Fig. 2a–c). Other aspects of J-RGCs were not detectably affected: dendritic field area, total length, and ventral asymmetry of the dendritic arbor did not differ significantly between controls and mutants (two-tailed Student's *t* test, $P = 0.62$, $P = 0.40$, $P = 0.39$, respectively; Fig. 2d and Supplementary Fig. 4a–c). The projection of axons to a primary central target, the superior colliculus, was similarly restricted to the superficial retinorecipient lamina in mutants and controls[30] (Supplementary Fig. 4d). Finally, Tbr1 mutant J-RGCs neither expressed markers of other RGC types, such as FoxP2, Satb1, or Tbr2[9,14–17], nor did they lose markers expressed by wild-type J-RGCs, such as Brn3b and Rbpms (Supplementary Fig. 4e; see also Supplementary Fig. 9b). Thus, Tbr1 plays a selective role in specifying the laminar position of J-RGC dendrites.

The ability to control the timing of Tbr1 deletion in *Tbr1^{J}* mice allowed us to determine when it is required for patterning J-RGC dendrites. J-RGC dendrites begin to extend around P0, are concentrated in the outer half of the IPL by P3, and become restricted to S1 by P6[28] (Supplementary Fig. 5a). Deletion at E14.5 and P0 perturbed dendritic lamination to a similar extent (compare Fig. 2b and Supplementary Fig. 4e), indicating that Tbr1 acted during rather than before dendritogenesis. Moreover, mutant J-RGCs extended ectopic dendritic branches within the inner half of the IPL by P4, indicating that Tbr1 acted during the period of laminar restriction ($P = 0.00018$, Cochran–Armitage test; Supplementary Fig. 5b,c). In contrast, deleting Tbr1 at P6 had no detectable effect on dendritic morphology ($P = 0.096$, Cochran–Armitage test; Fig. 2e and Supplementary Fig. 5d,e). Thus, Tbr1 was required to direct dendritic stratification rather than to maintain it.

To find out whether Tbr1 serves a similar role in other RGC types, we extended the analysis to α-OFF-s-RGCs. We could not use the TYW7 line for this purpose because Cre deletes its YFP cassette[22]. We therefore used the YFP-H line[25] to reveal dendritic morphology and identified α-OFF-s-RGCs as Opn$^+$ RGCs that lacked Brn3c and Tbr2, which are expressed by other alpha types[23]. As expected, dendrites of α-OFF-s-RGCs marked in this way arborized within S1 in control mice (Fig. 2f,h). In contrast 70% of these RGCs sent dendritic branches to S4 or S5 in *Tbr1$^{ret/ret}$;YFP-H* mice ($P = 1.6 \times 10^{-6}$, Pearson's χ^2 test; Fig. 2g,h). As was the case for J-RGCs, dendritic field area and length were unaffected ($P = 0.75$ and $P = 0.18$, respectively, two-tailed Student's *t* test; Supplementary Fig. 4f,g). Although we were unable to assay Tbr1-S1- and Tbr1-S2-RGCs, this result suggests a common role for Tbr1 in patterning dendritic lamination for all Tbr1-RGC types.

Loss of visual responses in Tbr1 mutant RGCs. Assessing the role of Tbr1 in RGC function required recording from Tbr1-RGCs. We faced two problems. First, in previous studies, we used transgenic expression of YFP to target cells for intracellular recording[6,9,10]. In this case, however, we were unable to identify Tbr1-RGCs prospectively. We therefore developed a calcium imaging protocol in which we expressed the calcium indicator GCaMP6f in a large fraction of RGCs, recorded responses to visual stimuli, and then performed immunostaining to identify individual types (Fig. 3a and Supplementary Fig. 6a–d). Second, identification initially relied on Tbr1 immunostaining, which was not applicable to *Tbr1$^{ret/ret}$*. We therefore used alternative markers. This approach was most successful for α-OFF-s-RGCs because, as noted above, these cells express Opn but not Brn3c or Tbr2.

We first characterized α-OFF-s-RGCs marked with the Tbr1-Opn and Tbr2-Opn-Brn3c combinations. In both cases, RGCs showed the expected properties[23,24]. They generated a robust increase in GCaMP signal to light offset and a decreased signal to

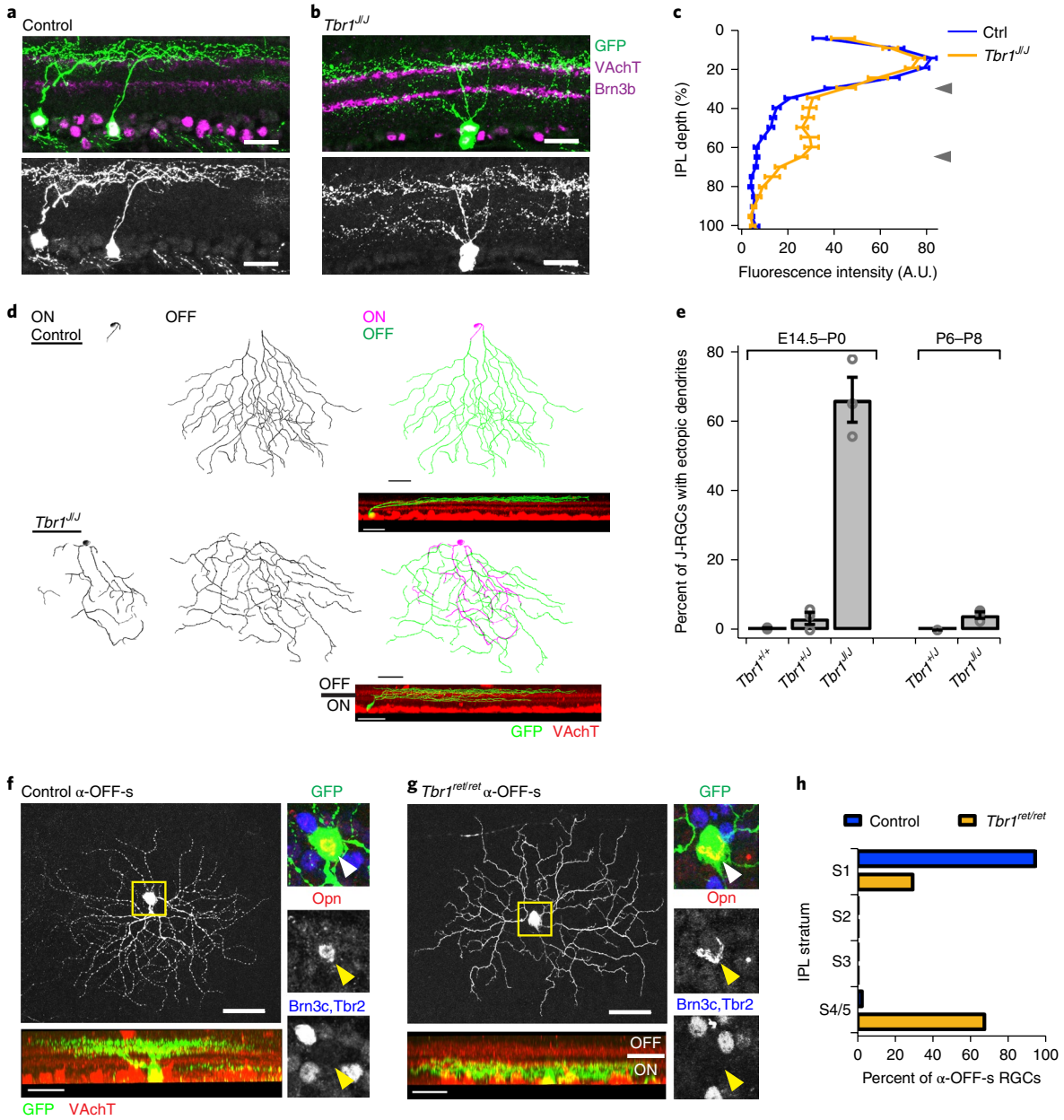

Fig. 2 | Tbr1 deletion results in ectopic dendritic lamination. a,**b**, Cross-sections of the IPL showing dendritic stratification of P20 J-RGCs in control and *Tbr1*$^{J/J}$ retina. Scale, 25 µm. Experiment was repeated independently in 4 animals per genotype with similar results. **c**, Distribution of GFP intensities from J-RGC dendrites through the depth of IPL in controls versus *Tbr1*$^{J/J}$ at P20 ($n = 20$ and 39 sections for control and *Tbr1*$^{J/J}$ respectively; 4 animals per genotype). Line plots and brackets indicate averages and standard error; $P = 1.2 \times 10^{-6}$, Cochran–Armitage test. Arrowheads indicate peaks of VAchT signals at S2 and S4. **d**, Traces (scale, 30 µm) and rotated views (inset; scale, 20 µm) of P20 control and *Tbr1*$^{J/J}$ J-RGCs. Experiment was repeated independently in 3 animals per genotype with similar results. **e**, Proportions of J-RGCs with ectopic dendrites when Tbr1 deletion is induced at E14.5–P0 or P6–P8. Each bar represents average proportions ± standard error. Circles indicate individual retinas ($n = 3$ retinas per genotype, each retina from a different animal; for E14.5–P0, $n = 144$–517, 34–146, and 35–100 cells for *Tbr1*$^{+/+}$, *Tbr1*$^{+/J}$, and *Tbr1*$^{J/J}$, respectively. For P6–P8, $n = 184$–303 and 40–188 cells for *Tbr1*$^{+/J}$ and *Tbr1*$^{J/J}$, respectively). **f**,**g**, En face (scale, 50 µm) and side (scale, 40 µm) views of α-OFF-s-RGCs labeled in YFP-H control (**f**) and *YFP-H;Tbr1*$^{ret/ret}$ (**g**) retinas. Insets show how cells were identified as α-OFF-s-RGCs (Opn^{+}Brn3c^{-}Tbr2^{-}). Loss of Tbr1 retargeted their dendrites to ON sublaminae of IPL. Experiment was repeated independently in 6 control and 9 *Tbr1*$^{ret/ret}$ animals with similar results. **h**, Proportions of α-OFF-s-RGCs that laminate within each sublamina in the IPL ($n = 24$ and 29 cells from 6 control and 9 *Tbr1*$^{ret/ret}$ retinas respectively, each retina from a different animal; $P = 1.6 \times 10^{-6}$, Pearson's χ^2 test).

light onset (Fig. 3b,c,f,g). They also responded to moving bars, with inhibition when a bright bar entered the receptive field and excitation when it left. However, they showed similar responses to motion in all directions and thus were not direction-selective (Fig. 3d,e,h,i and Supplementary Fig. 6e,f).

In contrast, α-OFF-s-RGCs in *Tbr1*$^{ret/ret}$ responded poorly to both flashes and moving bars (Fig. 3j–m and Supplementary Fig. 6g). Some nonresponsive cells are expected in calcium imaging studies for technical reasons (see Methods), but most control α-OFF-s-RGCs (11 of 16) responded appropriately, whereas only 4 of 13 mutant cells were responsive by criteria described in Methods. Moreover, of the 4 responsive mutant α-OFF-s-RGCs, only one appeared normal; the other 3 generated ON responses (Fig. 3j), a behavior not observed in control α-OFF-s-RGCs. Overall, however,

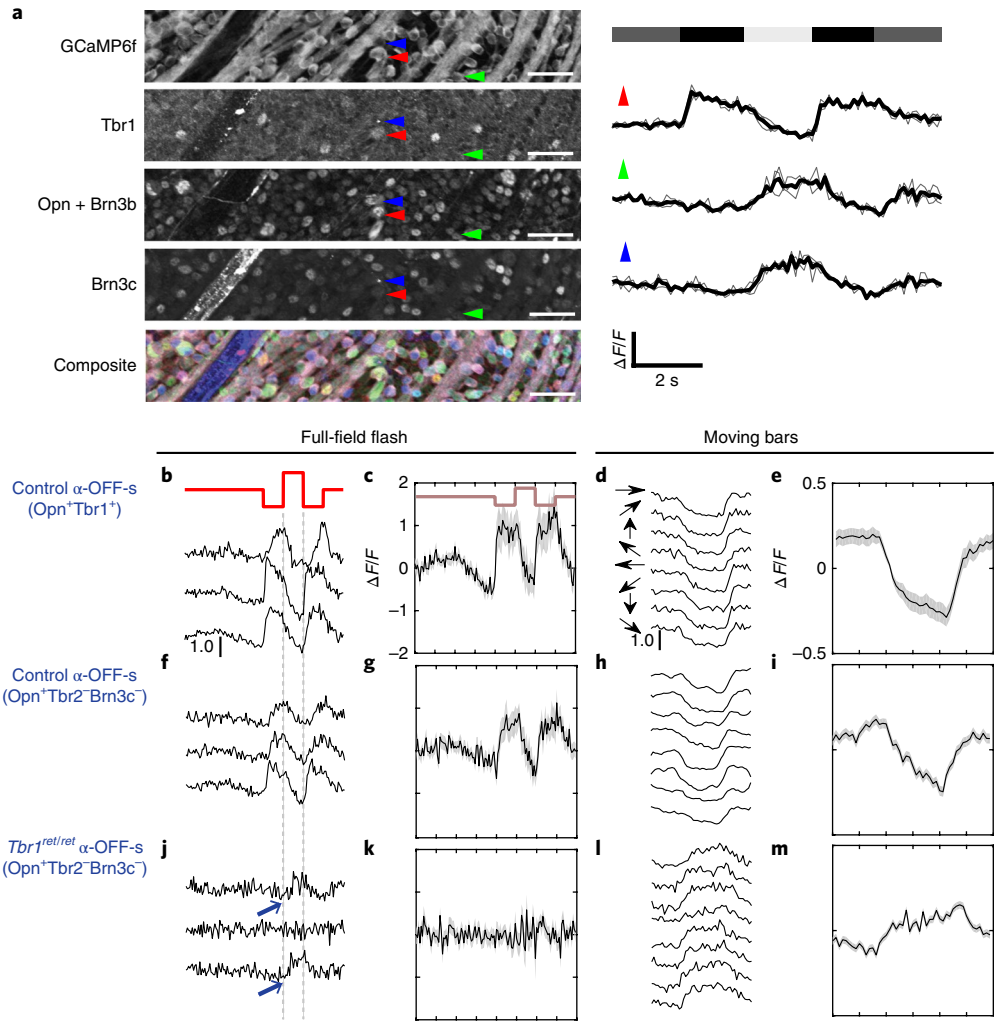

Fig. 3 | Physiological defects in Tbr1 mutants. a, Left: whole-mount view of a recorded field from a GCaMP6f-expressing retina that was immunostained for GFP, Tbr1, Opn + Brn3b, and Brn3c. Colors in composite image represent the above markers in gray, red, green, and blue, respectively. Right: calcium responses to a full-field flash from the three cells marked in **a**. Thick lines are averages of three repetitions, each represented by a thin line. Red arrow marks α-OFF-s-RGC (Tbr1$^+$Opn$^+$); as expected, it shows sustained activation to decreases in light intensity (top bar). Scale, 50 μm. **b**–**m**, Responses of α-OFF-s-RGCs in control and *Tbr1*$^{ret/ret}$. Scale, 100% Δ*F*/*F*. Shaded bounds indicate standard error. (**b**,**f**,**j**) Sample calcium responses evoked by a 2-s full-field flash (in red) from three cells per genotype. Responses are average of three repetitions. (**c**,**g**,**k**) Averaged responses of all cells to full-field flashes. Black line and shaded bounds represent mean ± s.e.m. (**d**,**h**,**l**) Sample calcium responses evoked by a bar moving in eight different directions. Responses are average of three presentations of the bar stimulus. (**e**,**i**,**m**) Averaged calcium responses to moving bars. Black line and shaded bounds represent mean ± s.e.m. **b**–**e** are control α-OFF-s-RGCs identified by Tbr1 and Opn (n = 18 cells from 6 retinas). **f**–**i** are control α-OFF-s-RGCs identified by Opn and absence of Tbr2 and Brn3c (n = 16 cells from 3 retinas). **j**–**m** are α-OFF-s-RGCs from *Tbr1*$^{ret/ret}$, identified as in **f**–**i** (n = 13 cells from 6 retinas).

the responsiveness of control and Tbr1 mutant RGCs were similar, suggesting that the defect was specific (Supplementary Fig. 6h,i). These results indicate that Tbr1 is required for the visual responsiveness of RGCs that express it. We speculate that this phenotype is a consequence of dendritic displacement, a possibility supported by the acquisition of ON responses in conjunction with the formation of ON arbors. It is also possible, however, that Tbr1 plays additional roles in responsiveness or synaptogenesis (see Discussion).

Tbr1 is sufficient for laminar specification of dendrites. To ask whether Tbr1 expression is sufficient to direct RGC arbors to the outer portion of the IPL, we ectopically expressed it by electroporation in neonatal retinas, along with a plasmid encoding a fluorescent protein (XFP) to mark transfected cells. This technique transfects multiple retinal cell types, including photoreceptors, interneurons, and RGCs, depending on the site of DNA delivery (see Methods). To transfect RGCs, we delivered DNA intraretinally. Nearly all RGCs transfected with Tbr1 + XFP elaborated dendrites within the OFF part of the IPL, whereas dendrites of control RGCs, transfected with XFP only, were equally likely to be found in OFF or ON regions ($P = 8.0 \times 10^{-7}$, Pearson's χ^2 test; Fig. 4a–c). Since only 15% of RGCs are endogenously Tbr1$^+$, it seemed likely that forced expression of Tbr1 redirected dendrites of RGCs from other sublaminae to S1. In support of this idea, dendrites of Tbr1-misexpressing RGCs were diverse in arborization patterns and sizes, as well as in levels of Brn3b (Supplementary Fig. 7a). Moreover, we found that dendrites of CART$^+$ ooDSGCs, which normally stratify in S2 and S4[31], were retargeted to S1 (Fig. 4b). Thus, Tbr1 plays an instructive role in dendritic lamination.

We also ectopically expressed Tbr1 in interneurons, using subretinal delivery of DNA. Tbr1-misexpressing interneurons similarly retargeted neurites to the outer IPL ($P = 1.0 \times 10^{-10}$,

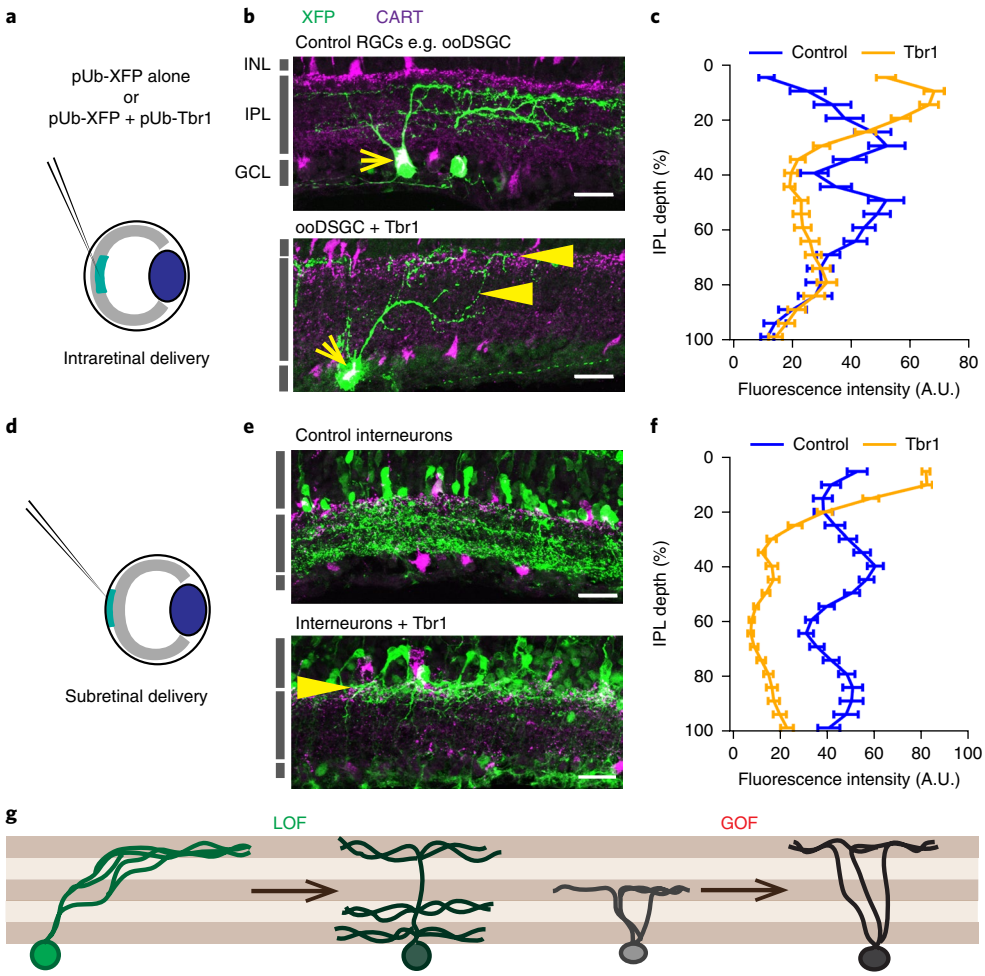

Fig. 4 | Ectopic expression of Tbr1 retargets neurites to the outer IPL. a, Intraretinal delivery of DNA for overexpression in RGCs. **b**, Expression of XFP alone (control) or XFP + Tbr1 into ooDSGCs, identified by CART immunoreactivity (yellow arrows). In **b** and **e**, yellow arrowheads mark neurites retargeted to the outer IPL. **c**, Quantification of dendrite lamination of control and Tbr1-misexpressing RGCs ($n = 39$ control cells from 6 retinas and 62 Tbr1-misexpressing cells from 7 retinas; $P = 7.95 \times 10^{-6}$, Pearson's χ^2 test). **d**, Subretinal delivery of DNA construct for overexpression in interneurons. **e**, Expression of XFP alone (control) or XFP + Tbr1 in interneurons. Scale, 25 µm. **f**, Quantification of neurite stratification within the IPL by control and Tbr1-misexpressing interneurons. Line plots and brackets in **c** and **f** indicate averages and standard errors ($n = 63$ and 65 sections from 8 control and 6 Tbr1-electroporated retinas respectively, $P = 1.0 \times 10^{-10}$, Cochran–Armitage test). **g**, Schematic summarizing loss- and gain-of-function (LOF and GOF, respectively) outcomes for Tbr1 within the IPL.

Cochran–Armitage test; Fig. 4d–f). The effect was specific, in that transfected somata remained in the inner nuclear layer and neither expressed RGC markers (for example, RBPMS) nor extended axons (Supplementary Fig. 7b,c). Amacrine cells that misexpressed Tbr1 also retained the characteristic marker AP2 (Supplementary Fig. 7d). Together, our loss- and gain-of-function approaches establish Tbr1 as a transcriptional determinant of laminar identity for RGC dendrites (Fig. 4g).

Tbr1 regulates Cdh8 and Sorcs3 expression in J-RGCs. To identify downstream effectors of Tbr1, we focused on J-RGCs, using five criteria to select promising candidates. First, we profiled J-RGCs by RNAseq at P6, when dendritic restriction is nearing completion, and compared them to profiles from two sets of ooDSGCs[9]. Second, we analyzed microarray data from seven groups of RGCs, including J-RGCs[18]. Third, from genes selectively expressed by J-RGCs in both comparisons, we chose those encoding cell-surface proteins, which are the most likely mediators of cell–cell interactions critical for patterning dendrites[7–10]. Fourth, of the 14 genes that fulfilled these criteria, we identified 6 that contained Tbr1-binding sites in their genomic loci as determined by chromatin-immunoprecipitation sequencing (ChIP-seq) of embryonic cortex[32]: *Alcam*, *Cdh8*, *Jam2*, *Neo1*, *Smo*, and *Sorcs3* (Fig. 5a). Of these 6 genes, *Cdh8*, a classical cadherin, and *Sorcs3*, a neuronal type I transmembrane receptor[33], have the most Tbr1-binding sites (Fig. 5a and Supplementary Fig. 8a). Finally, we isolated wild-type and Tbr1 mutant J-RGCs and compared them by RNAseq. Thirteen cell surface molecules were significantly downregulated in Tbr1-mutant J-RGCs ($P < 0.001$, two-tailed Fisher's exact test), including *Sorcs3*, *Jam2*, and *Cdh8*, but not *Alcam*, *Neo1*, or *Smo* (Supplementary Fig. 9a; see also Supplementary Fig. 8b,c). None of the remaining 10 candidates were selectively expressed by J-RGCs (Supplementary Fig. 9c), and analysis of *Jam2*-null mutants revealed subtle defects in dendritic morphology but no alterations in lamination[28]. Based on these considerations, we analyzed *Sorcs3* and *Cdh8* further.

We first validated that Sorcs3 and *Cdh8* expression in the retina are Tbr1-dependent by performing reverse-transcription quantitative PCR (RT-qPCR) on total RGCs isolated from P4 control and *Tbr1*$^{ret/ret}$ mutants: mRNA levels of both *Sorcs3* and *Cdh8* decreased by ~80% in mutants (Fig. 5b). We also immunostained control and Tbr1 mutant retinas for Sorcs3 and, lacking appropriate antibodies to Cdh8, visualized *Escherichia coli* beta-galactosidase (LacZ) driven

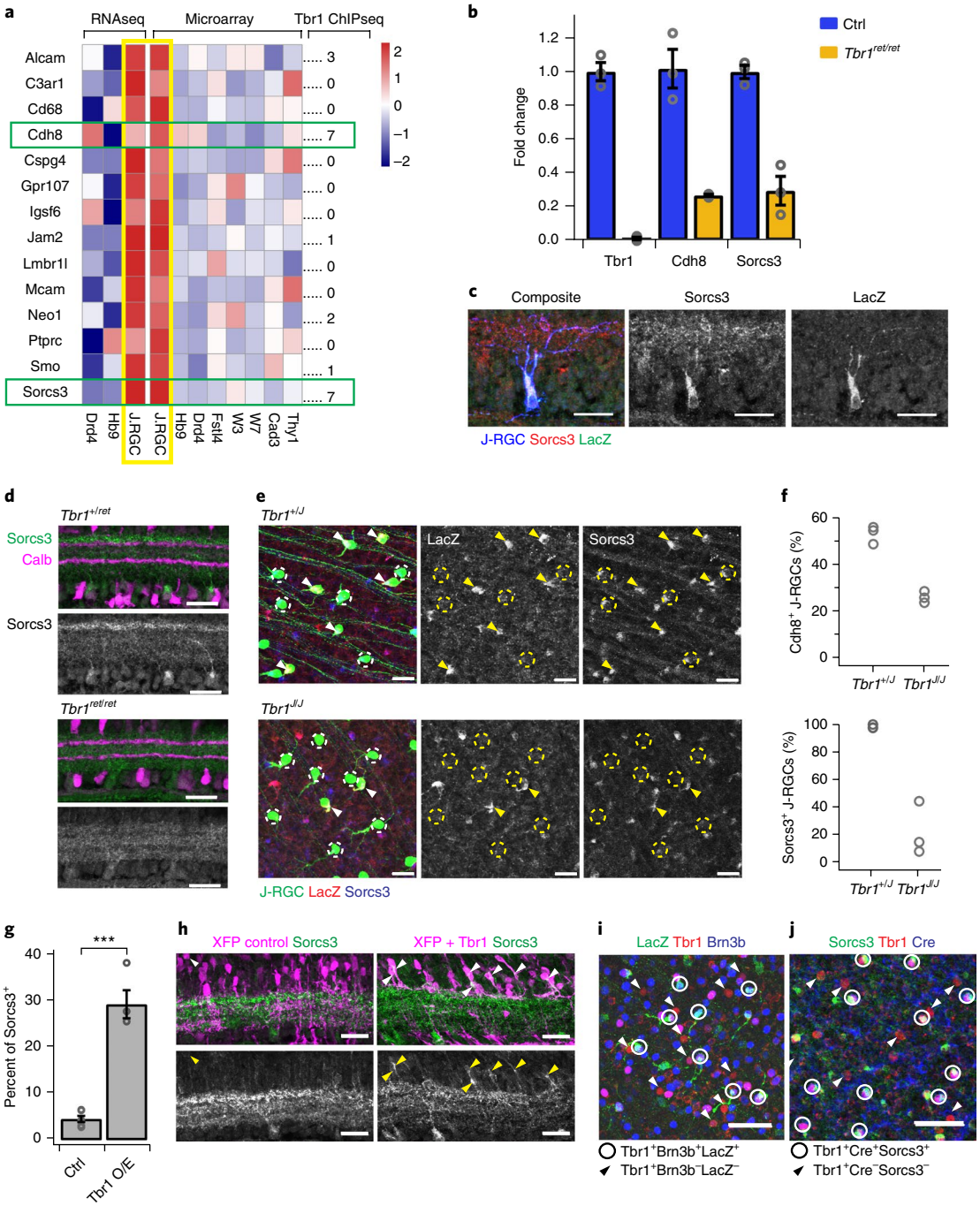

Fig. 5 | Cdh8 and Sorcs3 are Tbr1 targets in J-RGCs. a, Heatmaps showing expression of J-RGC-enriched cell-surface molecules from RNAseq and microarray data, and number of Tbr1-ChIPseq peaks associated with each gene[32] ($n=2$ litters of pups per RGC type). **b**, Expression of J-RGC candidate genes in P4 RGCs from *Tbr1*$^{ret/ret}$ mice relative to controls by RT-qPCR ($n=3$ animals per genotype); bars indicate mean ± standard error, circles indicate values from individual animals. **c**, Retinal cross-section showing expression of Sorcs3 and LacZ from the Cdh8^{LacZ} allele by a P5 J-RGC. **d**, Cross-section of control and *Tbr1*$^{ret/ret}$ IPL stained for Sorcs3. In controls, immunoreactivity is concentrated in a subset of RGC somata and dendrites in outer IPL. Levels are decreased in *Tbr1*$^{ret/ret}$. **e**, En face views of P4 J-RGC soma in *Tbr1*^{J} cells immunostained for Sorcs3 and LacZ. Arrowheads mark J-RGCs that express both markers. Dotted circles mark J-RGCs with no detectable LacZ: these cells still express Sorcs3 in *Tbr1*$^{+/J}$ but not in *Tbr1*$^{J/J}$ cells. **f**, Proportions of P4 J-RGCs that express LacZ or Sorcs3 in *Tbr1*^{J} retinas ($n=3$ retinas per genotype, 65–683 control cells and 152–520 and *Tbr1*$^{J/J}$ cells; $P=0.00050$ and $P=0.0025$ for LacZ and Sorcs3, respectively, two-tailed Student's *t* test). Circles represent individual retinas. **g**, Proportion of control (Ctrl) or Tbr1-misexpressing (Tbr1 O/E) interneurons that express Sorcs3 ($n=6$ control and 4 Tbr1-misexpressing retinas, 38–603 and 60–230 cells respectively, $^{***}P<9.9\times10^{-6}$, two-tailed Student's *t* test). Bars and brackets indicate mean ± standard error; circles represent individual retinas. **h**, Retinal cross-sections showing Sorcs3 expression in control and Tbr1-misexpressing interneurons. Arrowheads mark Sorcs3^{+} soma. Each experiment was repeated independently in 6 control and 4 Tbr1-misexpressing animals with similar results. **i**, Whole-mount of P3 Cdh8^{LacZ} retina stained for LacZ, Tbr1, and Brn3b. Circles mark J-RGCs that are triple-positive. Arrowheads mark the other Tbr1-RGC types, which are Brn3b^{-}. These cells lack LacZ immunoreactivity. **j**, Whole-mount of P5 JAM-B Cre knock-in retina stained for Sorcs3, Tbr1, and Cre. Dotted circles mark J-RGCs that are triple-positive. Arrowheads mark the other Tbr1-RGC types that are Cre^{-}. These cells do not express Sorcs3. Scale in **c**–**e**,**h**, 25 µm; in **i**,**j**, 50 µm. Each experiment in **c**–**e** and **i**,**j** was repeated independently in three animals with similar results.

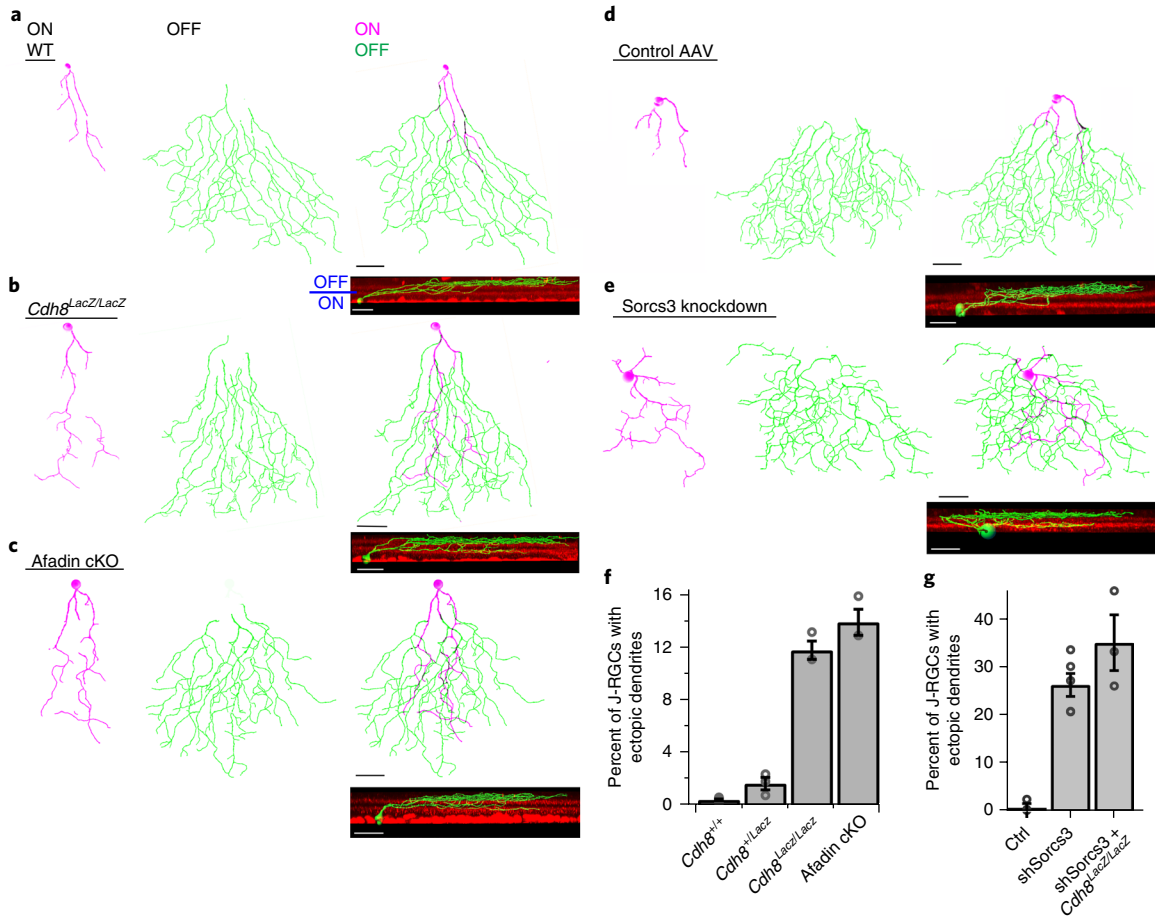

Fig. 6 | Requirement of Cdh8 and Sorcs3 for laminar restriction in J-RGCs. a–c, Traces of J-RGC dendrites in (**a**) wild-type (WT), (**b**) *Cdh8*$^{LacZ/LacZ}$ and (**c**) afadin conditional knock-out (cKO) retinas. Arbors in ON (magenta) and OFF (green) halves of the IPL are shown separately. Insets show rotated views. **d**,**e**, En face and rotated views of single-cell trace of a P12 J-RGC infected at P0 with a TdT control AAV (**d**) or AAV expressing a short hairpin RNA against Sorcs3 (*shSorcs3*) (**e**). Scale bars, 30 µm for en face view; 20 µm for rotated view. **f**, Proportion of J-RGCs with ectopic dendrites in each genotype ($n=5$ *Cdh8*$^{+/+}$, 3 *Cdh8*$^{+/-}$, 3 *Cdh8*$^{-/-}$, and 3 afadin cKO retinas; $P=8.7\times10^{-9}$, $F_{3,10}=163$, one-way ANOVA; $P=0.38$ for *Cdh8*$^{+/+}$ vs. *Cdh8*$^{+/LacZ}$ and $P=0.11$ for *Cdh8*$^{LacZ/LacZ}$ vs. afadin cKO; $P=1.4\times10^{-7}$, $P=2.8\times10^{-8}$, $P=1.2\times10^{-6}$, and $P=2.0\times10^{-7}$ for *Cdh8*$^{+/+}$ vs. *Cdh8*$^{LacZ/LacZ}$, *Cdh8*$^{+/+}$ vs. afadin cKO, *Cdh8*$^{+/LacZ}$ vs. *Cdh8*$^{LacZ/LacZ}$ and *Cdh8*$^{+/LacZ}$ vs. afadin cKO, respectively, Tukey–Kramer test). **g**, Proportion of J-RGCs with ectopic dendrites in retinas infected with AAV encoding TdT (Ctrl) or *shSorcs3* ($n=3$, 5, and 3 retinas, respectively, for control, *shSorcs3* and *shSorcs3* + *Cdh8*$^{LacZ/LacZ}$; $P=0.0013$, $F_{2,8}=17.2$, one-way ANOVA; $P=0.0048$, $P=0.0013$, and $P=0.25$ for ctrl vs. *shSorcs3*, ctrl vs. *shSorcs3* + *Cdh8*$^{LacZ/LacZ}$, and *shSorcs3* vs. *shSorcs3* + *Cdh8*$^{LacZ/LacZ}$, respectively, Tukey–Kramer test). In **f** and **g**, circles indicate data from individual retinas of different animals; bars and brackets represent mean and standard error.

from a *Cdh8*^{LacZ} knock-in allele[10]. Control J-RGCs at P4–P5 expressed both Sorcs3 and Cdh8 (Fig. 5c). However, while we detected Sorcs3 protein in all J-RGCs, we detected LacZ in only about half of them (Fig. 5d–f). In *Tbr1*$^{J/J}$ J-RGCs, levels of both Sorcs3 and LacZ protein were strongly reduced by P4–P5 ($P=0.0025$ and $P=0.00050$, respectively, two-tailed Student's *t* test; Fig. 5d–f). In the converse experiment, overexpression of Tbr1 by electroporation resulted in the upregulation of Sorcs3 protein in ~30% of Tbr1-misexpressing cells ($P<9.9\times10^{-6}$, two-tailed Student's *t* test; Fig. 5g,h). Together, these results confirm that Sorcs3 and Cdh8 expression in J-RGCs were regulated by Tbr1.

During the first postnatal week, neither Cdh8 nor Sorcs3 was detectably expressed by Tbr1-RGCs other than J-RGCs (Fig. 5i,j and Supplementary Fig. 8g). During the second postnatal week, however, their expression patterns diverged. Cdh8 expression declined in RGCs (Supplementary Fig. 8d) but was upregulated in OFF cone bipolar cells, as described previously[10]. Sorcs3, in contrast, was upregulated in rod bipolar cells and other RGCs (Supplementary Fig. 8e,f). Notably, Sorcs3 was concentrated within the dendrites of both RGCs and rod bipolar cells (Fig. 5d and Supplementary Fig. 8e).

Cdh8 and Sorcs3 pattern J-RGC dendrites. We used loss- and gain-of-function strategies to ask whether Cdh8 and/or Sorcs3 affect dendritic targeting of J-RGCs. To delete *Cdh8*, we used the *Cdh8*^{LacZ} line, which carries a null allele. Twelve percent of J-RGCs in *Cdh8*$^{LacZ/LacZ}$ retinas displayed ectopic ON dendrites that resembled those in Tbr1 mutant J-RGCs, while <1% of wild-type J-RGCs and <2% of *Cdh8*$^{LacZ/+}$ RGCs had ectopic dendrites ($P=1.4\times10^{-7}$ for wild-type vs. *Cdh8*$^{LacZ/LacZ}$ RGCs and $P=0.38$ for wild-type vs. *Cdh8*$^{+/LacZ}$ RGCs, Tukey–Kramer test; Fig. 6a,b,f). Given that Cdh8 was lost from all cells, we determined, in two ways, whether the ectopic dendrites were due to the specific loss from J-RGCs or were a secondary consequence of defects in other cells. First, we confirmed that other OFF-type RGCs, including α-OFF-s-RGCs, which express Tbr1 but not Cdh8, were not significantly affected in Cdh8 mutants ($P=0.12$, Cochran–Armitage test; Supplementary Fig. 10a,b). Second, we used the JAM-B-CreER line to selectively delete afadin, an actin-filament binding protein that interacts with cadherins[34], from J-RGCs; afadin mutants phenocopy cadherin mutants in some cases[35] (Duan et al., submitted). J-RGCs still formed ectopic dendrites, at a similar frequency to Cdh8 mutant

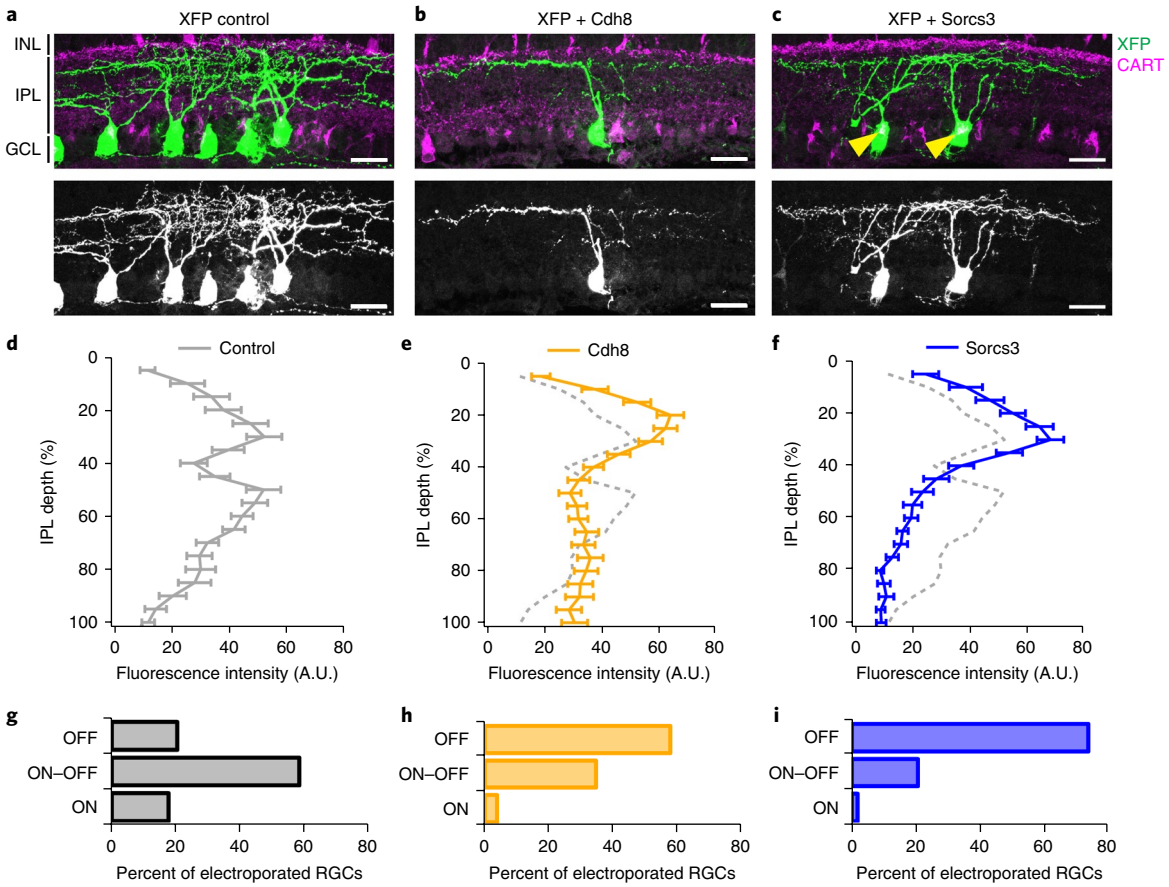

Fig. 7 | Ectopic expression of Cdh8 or Sorcs3 retargets RGC dendrites to the outer IPL. a–c, Retinal cross-section showing RGCs electroporated with control XFP (**a**), XFP + Cdh8 (**b**) or XFP + Sorcs3 (**c**). Arrowheads mark electroporated ooDSGCs, identified by their CART immunoreactivity. Scale, 25 µm. **d–f**, Distribution of fluorescence intensities from dendrites of (**d**) control RGCs (gray; replotted from Fig. 4c), (**e**) Cdh8-overexpressing RGCs (orange) or (**f**) Sorcs3-overexpressing RGCs (blue). Line plots and brackets indicate average and standard error. Similar results were observed in retinas from 6 control, 4 Cdh8-misexpressing and 5 Sorcs3-misexpressing retinas, each processed independently. **g–i**, Proportions of electroporated cells that extended OFF, ON-OFF or ON arbors in each condition ($n = 39$, 32, and 35 RGCs from 6 control, 4 Cdh8-misexpressing, and 5 Sorcs3-misexpressing retinas).

J-RGCs ($P = 0.11$ for $Cdh8^{LacZ/LacZ}$ vs. afadin conditional knock-out, Tukey–Kramer test; Fig. 6c,f). This result also suggests that the limited penetrance of the Cdh8 mutant is not a result of redundancy with or compensation by other cadherins.

Lacking a germline Sorcs3 mutant, we attenuated Sorcs3 expression using RNA interference, injecting intravitreally an adeno-associated virus (AAV) encoding a short hairpin RNA directed against Sorcs3 at P0 (Supplementary Fig. 10c–e). Dendrites of J-RGCs infected with a control AAV laminated appropriately (Fig. 6d,g), but ~30% of J-RGCs developed ectopic dendrites upon Sorcs3 knockdown, phenocopying the loss of Tbr1 ($P = 0.0048$, Tukey–Kramer test; Fig. 6e,g). Knocking down Sorcs3 was not significantly more effective in $Cdh8^{LacZ/LacZ}$ mice than in controls ($P = 0.25$, Tukey–Kramer test; Fig. 6g).

For gain-of-function analyses, we misexpressed Cdh8 or Sorcs3 in RGCs by neonatal electroporation. Control RGCs showed a similar preference for either the ON or OFF half of the IPL, as shown in the average of dendritic distributions from all electroporated RGCs (Fig. 7a,d), and they projected equally to ON and OFF sublamina (Fig. 7g). In contrast, Cdh8-misexpressing RGCs were on average biased to the OFF sublamina (Fig. 7b,e). Approximately 60% and 35% of Cdh8-misexpressing RGCs developed exclusively OFF dendrites or ON–OFF dendrites, respectively ($P = 0.0028$, Pearson's χ^2 test; Fig. 7h). Sorcs3-misexpressing RGCs showed an even stronger bias for the OFF sublamina (Fig. 7c,f). Of RGCs that overexpressed Sorcs3, 75% and 22% extended OFF and ON–OFF dendrites, respectively ($P = 4.5 \times 10^{-5}$, Pearson's χ^2 test; Fig. 7i). Affected RGCs included immunohistochemically labeled ooDSGCs (Fig. 7c). Therefore, both Cdh8 and Sorcs3 biased laminar targeting to the OFF half of the IPL.

Cdh8 and Sorcs3 act downstream of Tbr1. Finally, we asked whether restoration of Cdh8 or Sorcs3 in Tbr1 mutant J-RGCs would rescue laminar defects of their dendrites. We generated AAV vectors for this experiment because insufficient numbers of RGCs were transfected by electroporation. AAVs expressing Sorcs3, a Cdh8–RFP fusion, or RFP alone were injected intravitreally into $Tbr1^{f/f}$ animals at P0, and tamoxifen was delivered (also at P0) to delete *Tbr1* in J-RGCs and simultaneously label them with YFP. We then scored dendritic lamination of YFP^+ J-RGCs at P10. As in experiments presented above, ~60% of Tbr1 mutant J-RGCs labeled by the control AAV developed ectopic dendrites (Fig. 8a,d). In contrast, significantly fewer J-RGCs infected with Sorcs3- or Cdh8-expressing AAVs bore ectopic dendrites (11% for Sorcs3, 23% for Cdh8; $P < 0.0001$ for control vs. Sorcs3 or Cdh8, Tukey–Kramer test; Fig. 8b–d). Co-delivery of both Sorcs3 and Cdh8 almost completely rescued the Tbr1 phenotype (3%; $P < 0.0001$ for control vs. Sorcs3 + Cdh8, Tukey–Kramer test; Fig. 8d). Together, these data indicate that Cdh8 and Sorcs3 act downstream of Tbr1 to implement laminar identity of J-RGC dendrites.

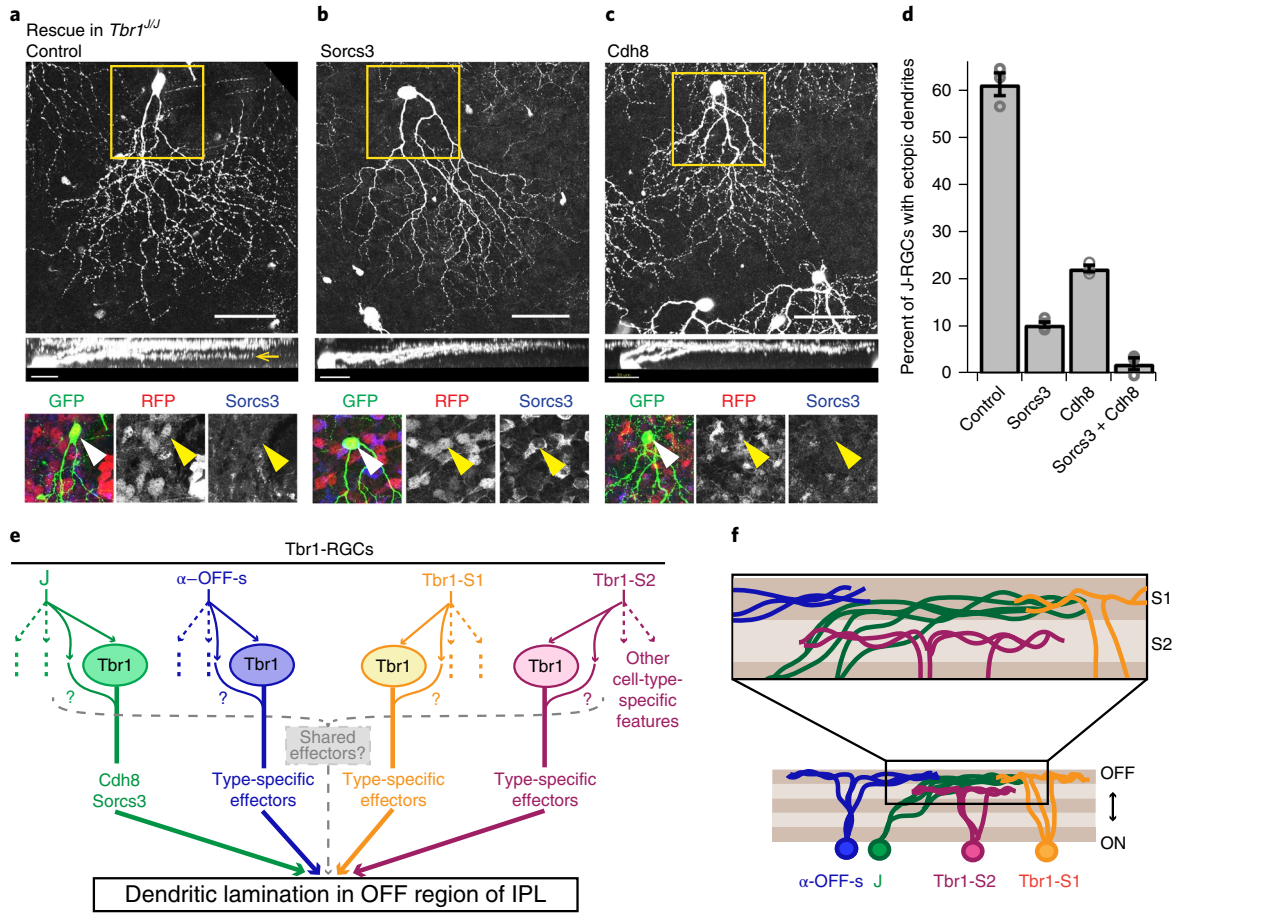

Fig. 8 | Regulation of dendrite laminar identity by Tbr1. a–**c**, En face (scale, 50 µm) and rotated (scale, 25 µm) views of Tbr1-mutant J-RGCs that had been infected with a control AAV (**a**), a Sorcs3-expressing AAV (**b**), or a Cdh8-expressing AAV (**c**). Sorcs3 was co-injected with RFP while Cdh8 was RFP-tagged. Yellow boxes mark insets, which show expression of AAVs and Sorcs3 protein in J-RGCs. As expected, Sorcs3 protein is lost from Tbr1-mutant J-RGCs infected with control or Cdh8 AAVs; it is restored in Sorcs3-infected J-RGCs (yellow arrowheads). Dendritic defects in Tbr1-deficient J-RGCs (**a**, yellow arrow) were rescued by either Sorcs3 (**b**) or Cdh8 (**c**). **d**, Proportions of J-RGCs with ectopic dendrites in *Tbr1*$^{J/J}$ retinas ($n = 3$ control, 4 Sorcs3, 3 Cdh8, and 3 Sorcs3 + Cdh8 infected animals; $P < 0.0001$, $F_{3,9} = 376$, one-way ANOVA; $P < 0.0001$ for control versus Sorcs3, Cdh8, or Sorcs3 + Cdh8, Tukey–Kramer test). **e**, Model of Tbr1-regulated laminar patterning. Solid colored arrows indicate molecular pathways that specify lamination. Dotted colored arrows indicate pathways for other cellular features. Arrows emanating from ovals marked 'Tbr1' indicate cell-type-specific effectors that bring dendrites to the OFF strata of the IPL, such as Cdh8 and Sorcs3 in the case of J-RGCs. Colored question marks indicate the hypothesis that Tbr1-independent mechanisms may act in parallel to Tbr1 to specify lamination. Dotted gray bracket and arrow indicate the possible presence of shared effectors for dendritic lamination that are commonly expressed by all four types. **f**, IPL schematic showing that all four Tbr1-RGC types laminate within the OFF half of the IPL (bottom), but differ in their precise lamination.

Discussion

The ability of different RGC types to respond selectively to certain visual features is a consequence of their synaptic inputs, key determinants of which are the IPL sublaminae in which their dendrites arborize. We demonstrate that a single transcriptional regulator can implement a common feature of dendritic laminar patterning by different RGC types. Tbr1 is expressed by four OFF-laminating RGC types, and it is both necessary and sufficient for laminar targeting of their dendrites within the IPL. We also identify two cell-surface molecules, Cdh8 and Sorcs3, as downstream effectors of Tbr1 in just one of the four types. Therefore, Tbr1 may instruct both a common laminar identity and subtle differences within that identity, in part by recruiting non-overlapping sets of effectors depending on cell type.

Tbr1 in neural development. Tbr1 belongs to a family of 17 related transcription factors (in mice) that share a conserved T-box DNA binding domain[36]. It is expressed in various neuronal populations in the vertebrate brain, including cerebral cortex and olfactory bulb[29,36–40], where it has been implicated in neuronal differentiation.

Tbr1 had not been studied in retina previously, to our knowledge, but much is known about its roles and expression in cortex. Our results document both similarities and differences between the two structures. Tbr1 is expressed exclusively by layer 6 pyramidal cells in cortex and RGCs in retina. Expression in both populations is initiated early but postmitotically, consistent with roles in neuronal development[36]. In cortical neurons, loss of Tbr1 disrupts migration, differentiation, and axonal targeting, and may result in a partial fate switch in which layer 6 pyramidal neurons assume layer 5 identity[39]. In contrast, Tbr1 has a notably selective effect on dendritic lamination in the retina, with no detectable role in fate determination, overall differentiation, or axonal projection.

Tbr2, the closest relative of Tbr1, is also expressed in both brain and retina. In cortex, expression of the two factors is sequential, with Tbr2 expressed in cortical progenitors and Tbr1 in layer 6 projection neurons[41]. In the retina, expression of both Tbr1 and Tbr2

persist into adulthood and, at least by late gestation (E17.5), is limited to non-overlapping groups of cells. Tbr2 is expressed by intrinsically photosensitive RGCs, which are distinct from Tbr1-RGCs, and is essential for their differentiation and/or survival[16,17]. Thus, despite their high homology, Tbr1 and Tbr2 appear to regulate distinct genes and processes depending on the brain region.

Laminar targeting by Cdh8 and Sorcs3. Using RNAseq, microarray, and ChIP-seq analyses, we chose Cdh8 and Sorcs3 as candidate mediators of Tbr1 effects in J-RGCs and confirmed that their expression is Tbr1-dependent. We do not know whether Tbr1 acts directly on these genes, but loss- and gain-of-function studies provided evidence that both act downstream of Tbr1.

Cdh8 is a member of the cadherin superfamily of adhesion molecules. Several type II cadherins have been implicated in shaping dendritic arbors of ooDSGCs and the axonal arbors of bipolar cells that innervate them[10] (Duan et al., submitted). Its role in J-RGCs was therefore not unexpected, but our demonstration that it acts downstream of Tbr1 provides the first clue as to how cadherin expression in the retina is regulated. Cdh8 is expressed transiently in J-RGCs, dissipating after P6, at which time dendritic restriction is complete (Supplementary Fig. 5a). Cdh8 is also expressed by type-2 bipolar cells, which arborize in S1[10], but it appears in these cells only after J-RGCs dendrites have become restricted. A homophilic interaction between arbors of these two cell types is therefore unlikely to explain the phenotype we observed. Instead, Cdh8 on J-RGCs is likely to interact with a heterophilic partner; one attractive possibility is Cdh11, to which it is known to bind[42].

Sorcs3 is a type I transmembrane protein that belongs to a family of vacuolar protein sorting 10 domain-containing receptors. Like other family members, Sorcs3 is expressed by a variety of neuronal populations[43,44]. Although other family members have been implicated in intracellular trafficking, much of the Sorcs3 protein is present on the cell surface[33]. Critically, Sorcs3 protein appears to be preferentially localized to neuronal dendrites. In hippocampus, Sorcs3 is present at dendritic spines, where it participates in the modulation of glutamate receptor function[44–46]. Similarly, it is concentrated in dendrites of J-RGCs. The identity of the ligand for Sorcs3 on J-RGC dendrites is unknown, but it binds nerve growth factor, raising the possibility that it engages neurotrophin signaling in retina.

It is likely that other transcriptional regulators act in parallel with Tbr1 and that other cell surface molecules act in parallel with Cdh8 and Sorcs3 to sculpt J-RGC dendrites. Indeed, the limited penetrance of the Tbr1, Cdh8, and Sorcs3 loss-of-function phenotypes supports this idea, although it is also possible that J-RGCs scored as 'normal' by our stringent criteria may have harbored subtle defects.

Regulators of dendrite targeting. Tbr1 expression is shared by four RGC types with dendrites that arborize in the outer third of the retina. Our loss- and gain-of-function methods confirm its role in laminar patterning of dendrites in at least two of these types and possibly in all four (Fig. 8e). It is possible that other cell types with a common lamination pattern may also express common transcription factors that specify their patterns. Indeed, several, including Tbr2, Satb1, and FoxP1[9,14,16,17], are expressed in multiple cell types that project to one or two common sublaminae in the IPL.

The approaches we have taken here suggest that lamination programs may converge upon single regulators like Tbr1 but diverge at the level of cell types. We identified Cdh8 and Sorcs3 as downstream targets of Tbr1, yet of the four Tbr1-RGC types, only J-RGCs express these genes at detectable levels during laminar patterning of dendrites. Since Tbr1 confers laminar identity on at least one other Tbr1-RGC type, the α-OFF-s-RGCs, Tbr1 must act through other effectors in those cells. By analogy to a scheme proposed to explain neuronal diversification and differentiation in *Caenorhabditis elegans*[47], factors that define overall identity of a RGC type may cooperate with Tbr1 to regulate unique sets of cell-surface molecules in each Tbr1-RGC type (Fig. 8e).

The engagement of at least partially non-overlapping sets of effectors in the Tbr1 types provides an explanation for the observation that precise dendritic lamination patterns within the outer third of the IPL differ across the four types, as though they interact with different cues (Fig. 8f). Alternatively or in addition, Tbr1-regulated cell-surface effectors may participate in the distinct synaptic choices each Tbr1-RGC type makes. The loss of visual responses from Tbr1 mutant α-OFF-s-RGCs is consistent with this idea.

Finally, Cdh8 and Sorcs3 are also Tbr1 targets in the cortex[32], and all three genes have been implicated as risk factors in behavioral disorders such as autism[48,49]. This conserved pathway is consistent with the speculation that dendritic defects contribute to the pathogenesis of diseases that result from neuronal miswiring.

Methods

Methods, including statements of data availability and any associated accession codes and references, are available at https://doi.org/10.1038/s41593-018-0127-z.

Received: 5 January 2018; Accepted: 20 February 2018;
Published online: 09 April 2018

References

1. Sanes, J. R. & Yamagata, M. Formation of lamina-specific synaptic connections. *Curr. Opin. Neurobiol.* **9**, 79–87 (1999).
2. Baier, H. Synaptic laminae in the visual system: molecular mechanisms forming layers of perception. *Annu. Rev. Cell Dev. Biol.* **29**, 385–416 (2013).
3. Sanes, J. R. & Masland, R. H. The types of retinal ganglion cells: current status and implications for neuronal classification. *Annu. Rev. Neurosci.* **38**, 221–246 (2015).
4. Famiglietti, E. V. Jr. & Kolb, H. Structural basis for ON-and OFF-center responses in retinal ganglion cells. *Science* **194**, 193–195 (1976).
5. Roska, B. & Werblin, F. Vertical interactions across ten parallel, stacked representations in the mammalian retina. *Nature* **410**, 583–587 (2001).
6. Krishnaswamy, A., Yamagata, M., Duan, X., Hong, Y. K. & Sanes, J. R. Sidekick 2 directs formation of a retinal circuit that detects differential motion. *Nature* **524**, 466–470 (2015).
7. Yamagata, M. & Sanes, J. R. Dscam and Sidekick proteins direct lamina-specific synaptic connections in vertebrate retina. *Nature* **451**, 465–469 (2008).
8. Yamagata, M. & Sanes, J. R. Expanding the Ig superfamily code for laminar specificity in retina: expression and role of contactins. *J. Neurosci.* **32**, 14402–14414 (2012).
9. Peng, Y. R. et al. Satb1 regulates Contactin 5 to pattern dendrites of a mammalian retinal ganglion cell. *Neuron* **95**, 869–883 (2017). e6.
10. Duan, X., Krishnaswamy, A., De la Huerta, I. & Sanes, J. R. Type II cadherins guide assembly of a direction-selective retinal circuit. *Cell* **158**, 793–807 (2014).
11. Matsuoka, R. L. et al. Transmembrane semaphorin signalling controls laminar stratification in the mammalian retina. *Nature* **470**, 259–263 (2011).
12. Sun, L. O. et al. On and off retinal circuit assembly by divergent molecular mechanisms. *Science* **342**, 1241974 (2013).
13. Kim, I. J., Zhang, Y., Yamagata, M., Meister, M. & Sanes, J. R. Molecular identification of a retinal cell type that responds to upward motion. *Nature* **452**, 478–482 (2008).
14. Rousso, D. L. et al. Two pairs of ON and OFF retinal ganglion cells are defined by intersectional patterns of transcription factor expression. *Cell Rep.* **15**, 1930–1944 (2016).
15. Sweeney, N. T., James, K. N., Nistorica, A., Lorig-Roach, R. M. & Feldheim, D. A. Expression of transcription factors divides retinal ganglion cells into distinct classes. *J. Comp. Neurol.* **520**, 633–655 (2017).
16. Mao, C. A. et al. T-box transcription regulator Tbr2 is essential for the formation and maintenance of Opn4/melanopsin-expressing intrinsically photosensitive retinal ganglion cells. *J. Neurosci.* **34**, 13083–13095 (2014).
17. Sweeney, N. T., Tierney, H. & Feldheim, D. A. Tbr2 is required to generate a neural circuit mediating the pupillary light reflex. *J. Neurosci.* **34**, 5447–5453 (2014).
18. Kay, J. N., Chu, M. W. & Sanes, J. R. MEGF10 and MEGF11 mediate homotypic interactions required for mosaic spacing of retinal neurons. *Nature* **483**, 465–469 (2012).
19. Rockhill, R. L., Euler, T. & Masland, R. H. Spatial order within but not between types of retinal neurons. *Proc. Natl Acad. Sci. USA* **97**, 2303–2307 (2000).

20. Rodieck, R. W. The density recovery profile: a method for the analysis of points in the plane applicable to retinal studies. *Vis. Neurosci.* **6**, 95–111 (1991).
21. Trenholm, S., Johnson, K., Li, X., Smith, R. G. & Awatramani, G. B. Parallel mechanisms encode direction in the retina. *Neuron* **71**, 683–694 (2011).
22. Kim, I. J., Zhang, Y., Meister, M. & Sanes, J. R. Laminar restriction of retinal ganglion cell dendrites and axons: subtype-specific developmental patterns revealed with transgenic markers. *J. Neurosci.* **30**, 1452–1462 (2010).
23. Krieger, B., Qiao, M., Rousso, D. L., Sanes, J. R. & Meister, M. Four alpha ganglion cell types in mouse retina: Function, structure, and molecular signatures. *PLoS One* **12**, e0180091 (2017).
24. Pang, J. J., Gao, F. & Wu, S. M. Light-evoked excitatory and inhibitory synaptic inputs to ON and OFF alpha ganglion cells in the mouse retina. *J. Neurosci.* **23**, 6063–6073 (2003).
25. Feng, G. et al. Imaging neuronal subsets in transgenic mice expressing multiple spectral variants of GFP. *Neuron* **28**, 41–51 (2000).
26. Bleckert, A., Schwartz, G. W., Turner, M. H., Rieke, F. & Wong, R. O. Visual space is represented by nonmatching topographies of distinct mouse retinal ganglion cell types. *Curr. Biol.* **24**, 310–315 (2014).
27. Bassett, E. A. & Wallace, V. A. Cell fate determination in the vertebrate retina. *Trends Neurosci.* **35**, 565–573 (2012).
28. Liu, J. & Sanes, J. R. Cellular and molecular analysis of dendritic morphogenesis in a retinal cell type that senses color contrast and ventral motion. *J. Neurosci.* **37**, 12247–12262 (2017).
29. Bulfone, A. et al. An olfactory sensory map develops in the absence of normal projection neurons or GABAergic interneurons. *Neuron* **21**, 1273–1282 (1998).
30. Hong, Y. K., Kim, I. J. & Sanes, J. R. Stereotyped axonal arbors of retinal ganglion cell subsets in the mouse superior colliculus. *J. Comp. Neurol.* **519**, 1691–1711 (2011).
31. Kay, J. N. et al. Retinal ganglion cells with distinct directional preferences differ in molecular identity, structure, and central projections. *J. Neurosci.* **31**, 7753–7762 (2011).
32. Notwell, J. H. et al. TBR1 regulates autism risk genes in the developing neocortex. *Genome Res.* **26**, 1013–1022 (2016).
33. Willnow, T. E., Petersen, C. M. & Nykjaer, A. VPS10P-domain receptors - regulators of neuronal viability and function. *Nat. Rev. Neurosci.* **9**, 899–909 (2008).
34. Takai, Y., Ikeda, W., Ogita, H. & Rikitake, Y. The immunoglobulin-like cell adhesion molecule nectin and its associated protein afadin. *Annu. Rev. Cell Dev. Biol.* **24**, 309–342 (2008).
35. Beaudoin, G. M. III et al. Afadin, a Ras/Rap effector that controls cadherin function, promotes spine and excitatory synapse density in the hippocampus. *J. Neurosci.* **32**, 99–110 (2012).
36. Mihalas, A. B. & Hevner, R. F. Control of neuronal development by T-box genes in the brain. *Curr. Top. Dev. Biol.* **122**, 279–312 (2017).
37. Hevner, R. F. et al. Tbr1 regulates differentiation of the preplate and layer 6. *Neuron* **29**, 353–366 (2001).
38. Han, W. et al. TBR1 directly represses Fezf2 to control the laminar origin and development of the corticospinal tract *Proc. Natl Acad. Sci. USA* **108**, 3041–3046 (2011).
39. McKenna, W. L. et al. Tbr1 and Fezf2 regulate alternate corticofugal neuronal identities during neocortical development. *J. Neurosci.* **31**, 549–564 (2011).
40. Huang, T. N. et al. Tbr1 haploinsufficiency impairs amygdalar axonal projections and results in cognitive abnormality. *Nat. Neurosci.* **17**, 240–247 (2014).
41. Englund, C. et al. Pax6, Tbr2, and Tbr1 are expressed sequentially by radial glia, intermediate progenitor cells, and postmitotic neurons in developing neocortex. *J. Neurosci.* **25**, 247–251 (2005).
42. Shimoyama, Y., Tsujimoto, G., Kitajima, M. & Natori, M. Identification of three human type-II classic cadherins and frequent heterophilic interactions between different subclasses of type-II classic cadherins. *Biochem. J.* **349**, 159–167 (2000).
43. Hermey, G. et al. The three sorCS genes are differentially expressed and regulated by synaptic activity. *J. Neurochem.* **88**, 1470–1476 (2004).
44. Oetjen, S., Mahlke, C., Hermans-Borgmeyer, I. & Hermey, G. Spatiotemporal expression analysis of the growth factor receptor SorCS3. *J. Comp. Neurol.* **522**, 3386–3402 (2014).
45. Breiderhoff, T. et al. Sortilin-related receptor SORCS3 is a postsynaptic modulator of synaptic depression and fear extinction. *PLoS One* **8**, e75006 (2013).
46. Christiansen, G. B. et al. The sorting receptor SorCS3 is a stronger regulator of glutamate receptor functions compared to GABAergic mechanisms in the hippocampus. *Hippocampus* **27**, 235–248 (2017).
47. Hobert, O. Terminal selectors of neuronal identity. *Curr. Top. Dev. Biol.* **116**, 455–475 (2016).
48. Huang, T. N. & Hsueh, Y. P. Brain-specific transcriptional regulator T-brain-1 controls brain wiring and neuronal activity in autism spectrum disorders. *Front. Neurosci.* **9**, 406 (2015).
49. De Rubeis, S. et al. Synaptic, transcriptional and chromatin genes disrupted in autism. *Nature* **515**, 209–215 (2014).

Acknowledgements

We thank Z. He and C. Wang at Boston Children's Hospital Viral Core for their generous support (5P30EY012196). This work was supported by NIH grants NS29169 and EY022073 to J.R.S., NS34661 to J.L.R., and MH094589 to B.C. J.L. was funded by an Agency for Science, Technology and Research (A*STAR) fellowship from Singapore.

Author contributions

J.L. and J.R.S. conceived the study, planned experiments, analyzed data, and wrote the paper. J.L. performed all experiments unless otherwise stated. J.D.S.R. performed and analyzed calcium imaging experiments. A.K. built instrumentation, wrote stimuli, and analyzed calcium imaging experiments. M.A.L. performed experiments on afadin, Cdh8, and axonal projections. S.P. generated cDNA libraries for Tbr1 wild-type and mutant J-RGCs. J.L.R.R. and B.C. generated conditional Tbr1 mutant mice.

Competing interests

The authors declare no competing interests.

Additional information

Supplementary information is available for this paper at https://doi.org/10.1038/s41593-018-0127-z.

Reprints and permissions information is available at www.nature.com/reprints.

Correspondence and requests for materials should be addressed to J.R.S.

Publisher's note: Springer Nature remains neutral with regard to jurisdictional claims in published maps and institutional affiliations.

Methods

Mice. A conditional Tbr1 mutant allele was generated at inGenious Targeting Laboratory (Ronkonkoma, NY). *LoxP* sites were inserted into introns 1 and 3, flanking *Tbr1* exons 2 and 3 (Fig. 2b). To enable selection of homologous recombinants, the *loxP* site in intron 3 was embedded in a *neo* cassette flanked by *Frt* sites. The *neo* cassette was removed by mating to Flp-expressing mice[50] to generate the *Tbr1*^{loxP} allele. Cre excision removed exons 2 and 3, including the T-box DNA binding region, similar to the *Tbr1* constitutive null allele[29].

The following mouse lines were generated in our laboratory and described previously: The *JAM-B-CreER* transgene was generated from a bacterial artificial chromosome by replacing the translational start site of *JAM-B* with a cDNA encoding a ligand-activated *Cre* recombinase, thereby placing the expression of CreER under the control of regulatory elements of *Jam2*[13]. *Thy1-STOP-YFP* expresses YFP in many neurons, including all RGCs, following Cre-mediated excision of sequences that terminate transcription and translation[51]. Thus, in *JAM-B-CreER;Thy1-STOP-YFP* double transgenics, the administration of tamoxifen results in labeling of J-RGCs. We used homologous recombination to generate a *JAM-B* Cre knock-in mouse, in which the first exon of the endogenous *Jam-2* gene has been replaced with the gene encoding Cre recombinase[28]. Thy1-YFP-H mice label a sparse, nearly random subset of RGCs[25]. In TYW7, Thy1 regulatory elements drive the expression of *loxP*-flanked *YFP*; Cre deletes the *YFP*[22]. The Cdh4-CreER knock-in line was generated by targeted insertion of a *frt-neo-frt* cassette, a 6×*myc*-tagged *CreER-T2* and polyadenylation signal at the translational start site of the *Cdh4* coding sequence[14].

A *Vglut2-Ires-Cre* knock-in line[52] was obtained from International Mouse Strain Resource (IMSR). *Rosa-CAG-lox-STOP-lox-GCaMP6f::deltaNeo*[53] (*loxP*-flanked *GCaMP6f*) and *HB9-GFP*, which label ooDSGCs that prefer ventral motion[21,54], were obtained from the Jackson Laboratory. Dopamine receptor D4-GFP (DRD4-GFP) mice, which label ooDSGCs that prefer nasal motion[31,55], were obtained from MMRRC-UNC. *Six3-cre* transgenic mice were provided by W. Klein (M.D. Anderson Cancer Center)[56]. Cdh8^{LacZ} were provided by M. Takeichi (Riken-CDB, Kobe, Japan)[10,57]. A conditional afadin mutant (afadin cKO) was obtained from L. Reichardt[35].

Tamoxifen (150 µg, Sigma) was injected subcutaneously into P0–P1 pups or intraperitoneally into P6–P8 pups and E14.5 pregnant females. Animals were killed by intraperitoneal injections of sodium pentobarbital followed by cervical dislocation. Animals below P10 were killed by cervical dislocation. Animals of either sex were analyzed. All mice were maintained on a C57BL/6 and CD1 mixed background. The numbers and ages of animals per experiment are indicated in figure legends. Animals were used in accordance with NIH guidelines and protocols were approved by the Institutional Animal Use and Care Committee at Harvard University.

Histology. Retinas were fixed in cold 4% PFA in PBS for 1.5 h. For sections, retinas were incubated with 30% sucrose in PBS for at least 2 h, frozen, and cryosectioned at 20 µm. Sections were then blocked with 5% normal donkey serum/0.3% Triton X-100/PBS for 30 min, and incubated with primary antibodies in 3% normal donkey serum/0.3% Triton X-100/PBS overnight. After two PBS washes, the sections were incubated with secondary antibodies for 2 h, washed and mounted in Fluoromount. For whole mounts, retinas were dissected free of sclera, blocked for at least 1 h, incubated in primary antibodies for 5–7 d, followed by secondary antibodies overnight. The retinas were then washed with PBS for at least 3–4 h and mounted in Vectashield. Following calcium imaging experiments, retinas were fixed in fresh cold 4% PFA for 75 min and 0.1% Triton X-100 used for all blocking and antibody solutions.

For analysis of central projections, animals were anesthetized with intraperitoneal injection of 60 mg/kg ketamine plus 7.5 mg/kg xylazine and transcardially perfused. Brains were fixed overnight in 4% PFA at 4 °C, washed with 1×PBS and sectioned sagittally at 70 µm on a vibratome. Sections were blocked for 2 h, incubated in primary antibodies for 48 h at 4 °C, washed three times with PBS at room temperature (20–25°) for at least 1 h, and re-incubated in secondary antibodies overnight. Sections were washed three times in PBS at room temperature over 1 h and mounted in Vectashield.

Antibodies used were as follows: chicken anti-GFP (1:1,000, Abcam ab13970), rabbit anti-Tbr1 (1:1,000, Abcam ab31940)[39], rabbit anti-Tbr2 (1:500, Abcam ab23345), goat FoxP2 (1:1,000, Abcam ab1307), guinea pig FoxP1 (1:5,000, Ben Novitch, UCLA), goat Satb1 (1:1,000, Santa Cruz Biotechnology sc-5989×), goat Pcsk2 (1:1,000, R&D Systems AF6018; Supplementary Fig. 4e) rabbit anti-mCherry (1:5,000)[58], mouse anti-Cre (1:500, Millipore MAB3120), goat anti-VAchT (1:1,000, Millipore ABN100), mouse anti-Brn3a (1:500, Millipore Mab1585), guinea pig anti-VAchT (1:500, Promega G4481), guinea pig Rbpms (1:500, PhosphoSolutions 1832-RBPMS), goat anti-Brn3b (1:500, Santa Cruz Biotechnology sc-6026), mouse anti-Brn3c (1:250, Santa Cruz Biotechnology sc-81980), rabbit anti-Calbindin (1:10,000, Swant CB38a), rabbit anti-CART (1:2,000, Phoenix Pharmaceuticals H-003-62), Syt2 (1:250, ZIRC Znp-1), goat anti-Opn (1:500, R&D Systems AF-808), goat Sorcs3 (1:1,000, R&D Systems AF3067; Fig. 5d), mouse PKCa (1:500, Abcam ab31), goat anti-Alcam (1:1,000, R&D Systems AF1172[59]), goat anti-Neo1 (1:1,000, R&D Systems AF1079; Supplementary Fig. 8c), and rabbit anti-β-galactosidase (1:5,000)[10]. Dylight 405-, Alexa Fluor 488-, Cy3- and Alexa Fluor 647-conjugated secondary antibodies (1:1,000) were obtained from Jackson ImmunoResearch. Unless stated otherwise, these antibodies have been previously validated[14].

In vivo electroporation. Tbr1 and Sorcs3 expression constructs were generated by PCR-amplifying the open reading frames from cDNA isolated from wild-type retinas and cloning them into an expression vector bearing the ubiquitin promoter. A Cdh8-mCherry fusion was obtained by restriction digest from the vector described in ref[10]. A fluorescence expression plasmid (GFP or mCherry) was either electroporated alone (as a control) or co-electroporated with Tbr1 or Sorcs3 into neonatal retinas (P0–P1) as previously described[60,61]. The Cdh8-mCherry plasmid was electroporated alone. Expression plasmids (~3 mg/mL) were injected intraretinally or into the subretinal space of P0 mice and current pulses (80 V, 50 ms) were applied across the head using paddle electrodes (Harvard Apparatus, size 9). Intraretinal injection was used to label RGCs[61]; only P0 pups were used and the glass needle was angled acutely such that it traversed as great a distance as possible within the retina. Subretinal injection labeled photoreceptors, interneurons, and Muller glia, but not RGCs[60]. Retinas were analyzed at P12–P14 unless otherwise stated. Retinas were taken at ≤P12 for analysis of Sorcs3 expression. For quantification of Sorcs3 expression in Tbr1-misexpressing cells, discrete cell somata with cytosolic Sorcs3 staining (perinuclear and/or in neurites) were counted as Sorcs3^{+}.

RNAseq and transcriptomic analysis. Fluorescently labeled J-RGCs were isolated from JAM-B-CreER×Thy1-STOP-YFP retinas by fluorescence-assisted cell sorting (FACS) at P6. Libraries were prepared using Ovation Ultralow System V2 1-16 (Nugen) and sequenced using Illumina NextSeq (75 cycles, single-end). Hb9-GFP and Drd4-GFP RNAseq were generated similarly[9]. Two biological replicates were generated for each RGC type. Data were analyzed using Tuxedo suite[62] and edgeR[63]. Reads were trimmed by Trimmomatic[64] and mapped onto the mouse genome (mm9 or mm10) by Tophat[62]. For analysis by Tuxedo suite, transcripts were counted using Cufflinks, and differentially expressed genes were detected with Cuffdiff. For analysis by edgeR, mapped reads were counted by HTSeq and counts per million total reads (CPM) generated on edgeR for differential analysis. Microarray data were obtained from a published dataset[18].

J-RGC enriched genes with $\log_2$ fold change >1 relative to Hb9-GFP and Drd4-GFP were compiled. Genes with $\log_2$(CPM) <2.32 were discarded. Genes with ontology terms associated with cell-surface membranes, excluding ion channels and enzymes, were shortlisted. The Genomic Regions Enrichment of Annotation Tool (GREAT)[65] was used to analyze a published Tbr1 ChIP-seq dataset[32]. Tbr1 ChIP-seq peaks were visualized on Integrative Genomics Viewer (IGV, Broad Institute).

P4–P5 Tbr1 wild-type and mutant J-RGCs were isolated by FACS in pools of 100 cells. We collected 11 samples: 5 samples from 4 wild-type mice and 6 samples from 4 *Tbr1*$^{f/f}$ mice. Smartseq2 and Nextera XT were used to prepare cDNA libraries[66]. Libraries were sequenced on Nextseq (75 cycles, single-end) and analyzed as described above.

Image and statistical analyses. Imaging was performed on Olympus FV1000 or Zeiss LSM-710 confocal microscopes using 405-, 488-, 568- and 647-nm lasers. Images were acquired at *x-y-z* resolution of 0.31 µm×0.31 µm×0.5–2 µm. Images were analyzed in ImageJ. Gamma and contrast settings of the images were adjusted to make dim features visible, without eliminating background signal. To quantify the location of J-RGC dendrites or laminar distributions of neurites from electroporated cells within the IPL, line scans were drawn across the entire IPL, and YFP intensity values across IPL depth were obtained using the ImageJ/Analyze/Plot Profile function. Depth values were normalized such that 0% indicates the INL–IPL border and 100%, the IPL–GCL border. Intensity values were normalized to the maximum intensity within each line scan. Intensity values, in arbitrary units, were binned for every 5% IPL depth and averaged across samples. Dendritic field areas were measured by drawing convex hulls around dendrites. The coverage factor was calculated as the product of dendritic field area and spatial density. Mosaic analysis was done on WinDRP software[18,19]. Dendrites were traced using Imaris 7.4.0. Dendrite length was obtained using Imaris or Simple Neurite Tracer on ImageJ 1.49 u. Statistical analyses were performed using Pearson's χ^2 tests, Cochran–Armitage tests, one-way ANOVA followed by Tukey–Kramer test or two-tailed Student's *t* tests, as described in figure legends, on Microsoft Excel or GraphPad Prism 7.03. Cochran–Armitage tests were used to assess the distribution of neurites across the IPL between two conditions, where the IPL was divided into equal bins and the order of bins fixed to reflect the arrangement of the IPL. Pearson's χ^2 tests were used when observations such as cell counts were categorized into discrete classes and the order of the classes was arbitrary. Average values are represented as mean ± standard error unless otherwise stated. No statistical methods were used to predetermine sample sizes, but our sample sizes are similar to those reported in previous publications[6,10,28]. Data distribution was assumed to be normal, but this was not formally tested. Samples were allocated by genotype or treatment (for example, different electroporation constructs or AAV injections). For experiments involving animals of the same genotype (for example, electroporation of wild-type pups), animals were randomly assigned to one treatment or another. Data collection and analysis were not performed blind to the conditions of the experiments. Exclusion criteria were pre-established for initial

characterization of calcium responses as detailed below. No other data or animals were excluded from analysis.

Reverse-transcription quantitative PCR (RT-qPCR). RGCs were isolated from P4 control and *Tbr1*$^{ret/ret}$ retinas by live-staining with microbeads conjugated to monoclonal anti-mouse CD90.2, followed by magnetic column purification (MACS Miltenyi Biotec). RNA was extracted using DirectZol RNA extraction kit (Zymo Research) and assessed on a Bioanalyzer. First-strand cDNA synthesis was performed on equal amounts of RNA using Superscript III reagents (Invitrogen). qPCR was performed using a KAPA Sybr FAST qPCR kit Master Mix (Kapa Biosystems) on ABI 7900. cDNA levels across samples were normalized using primers against *Hprt*. Fold-change expression relative to controls was calculated by the ΔΔCt method. Primers used were as follows: *Cdh8*, 5′-AACCAGATTTGCAGTTTATGCCA-3′ and 5′-TTGCCCATATCCACACGGTC-3′; *Hprt*[67], 5′-CAAACTTTGCTTTCCCTGGT-3′ and 5′-CAAGGGCATATCCAACAACA-3′; *Sorcs3*, 5′-CTCTCGGTGGTATTCGTCGG-3′ and 5′-CAATGCTTCCTATGACCCGC-3′; *Tbr1*[40], 5′-CAAGGGAGCATCAAACAACA-3′ and 5′-GTCCTCTGTGCCATCCTCAT-3′.

Intravitreal injections. The AAV construct encoding a shRNA against Sorcs3 was generated by replacing the shPTEN sequence in pAAV9-U6-shPTEN-CMV-mCherry[68] with *shSorcs3*. The efficacy of *shSorcs3* was tested in vitro on HEK293T cells that were transfected with a Sorcs3-expression plasmid. AAV9-cag-Td-tomato was used as a control. Animals were killed for analysis and retinas collected at least 2 weeks postinjection or, in the case of Sorcs3, by P12.

For the generation of Sorcs3- and Cdh8-expressing AAVs, an AAV backbone with an optimized expression cassette, containing a truncated WPRE and SV40 late polyadenylation signal[69], was used to accommodate the large sizes of these cDNAs. The GFP sequence in pAAV-CW3SL-EGFP (Addgene plasmid #61463) was first replaced with the sequence of *Sorcs3* or RFP-tagged *Cdh8*. Then, the CaMKIIa promoter was replaced with a synuclein promoter. AAVs were delivered intravitreally at P0 and retinas collected 10 d later for whole-mount processing.

AAVs to alter Cdh8 or Sorcs3 levels were generated by Boston Children's Hospital viral core. AAV9.Syn.GCaMP6f.WPRE.SV40 was purchased from the Penn Vector Core. We delivered ~0.5–1 µL of each AAV to each retina intravitreally. For adults, ophthalmic ointment was applied to the eye postinjection.

For visualizing axonal projections, 1 µL of fluorescently tagged recombinant cholera toxin subunit B (CTb) was injected into each eye using a 30.5-gauge Hamilton syringe. The contralateral superior colliculus and uninjected retina were collected 2 d after injection and processed for histology, as described above.

Calcium imaging. Mice were dark-adapted overnight before being killed for analysis. The retina was rapidly dissected under infrared illumination into oxygenated (95% O2; 5% CO2) Ames solution (Sigma). Three relaxing cuts were made and the retina was then placed in a recording chamber, ganglion cells facing up on the stage of a custom-built two-photon microscope[6]. We added 5–10 µL of 0.2 mg/mL sulforhodamine 101 (Sigma) to the recording chamber to label blood vessels, and the retina was left to rest for 5–10 min. GCaMP-expressing neurons were imaged under two photon illumination (wavelength = 960 nm) and stimulated with patterned visual stimuli delivered through the objective. Movies (700 × 100 pixels; 420 × 60 µm) were collected and then regions of interest (ROIs) drawn around individual cells to extract neural responses (see analysis below). To measure stimulus noise, retinas were presented with stimuli without laser activation. Stimulus-generated noise in our calcium imaging movies was worst at the edges of the scan pattern and was all but absent in the center.

Light stimuli were delivered through the objective from a modified DLP projector suspended above the microscope stage using a custom made lens subsystem, as described previously[70]. Monochrome light was used (wavelength = 405 nm, width = 10 nm), and the background intensity set to 4.2206×10^4 R*/rod/s. The LED was triggered on the edges of every linescan in order to restrict stimulus contamination to the edges of our calcium imaging movies. Visual stimuli were written in Matlab and displayed on the projector using the psychophysics toolbox. Patterns were binary, and gray was achieved by inverting a single-pixel checkerboard pattern on every frame. Moving bars were presented as a long bar moving along its long axis; the short axis of the bar corresponded roughly to the receptive field width of the recorded neuron; Bars moved with a velocity of 1,000 µm/s; their length was adjusted to give good separation between the leading and trailing edges.

Following recording, retinas were fixed, immunostained and imaged as described above. Regions of the confocal images that corresponded to the recorded field were located by reference to the pattern of blood vessels. Confocal images were aligned to recorded fields using the affine transform function on ImageJ. ROIs for cell bodies in the transformed image were drawn and molecular signatures were assigned to each cell.

Code written in Matlab R2015b was used to extract Ca^{2+} traces for each ROI. Traces were first de-trended using Matlab's moving mean function. The ROI for each cell was applied to the noise movie and the noise trace was subtracted from the response of that cell; this procedure allowed us to account for varying noise across our imaging field. Quality index and *z*-score were calculated as described previously[71]. The quality index provides a measure of consistency across trials. It is calculated as the variance of the mean response for all trials (generally 3), divided by the mean of the variance over trials. Thus, the index spans from 1/3, if all trials are completely random with respect to each other (but have the same variance), to 1 if all responses are identical. Nonresponsive cells tend to have low quality indices, because they are dominated by noise. The *z*-score of responses to stimuli, a more direct measure of responsiveness, was calculated with respect to the mean and s.d. of signals recorded during steady gray illumination that preceded the stimulus (8 s for full field flashes and 6 s for moving bars). For initial characterization (Supplementary Fig. 6a–d), we counted only cells with quality index > 0.45 and a *z*-score that was > 1.0 for at least two consecutive timepoints. For the analysis of α-OFF-s-RGCs in control versus *Tbr1*$^{ret/ret}$, these selection criteria were omitted and all immunohistochemically identified cells were analyzed, so that we could detect changes in responsiveness in *Tbr1* mutants.

Accession codes. GEO: J-RGC RNAseq data, GSE102888; Tbr1 wild-type and mutant J-RGC RNAseq, GSE108789.

Published gene sets used in this study are available at GEO accession codes GSE35077[18]; GSE71384[32]; GSE90673[9].

Reporting Summary. Further information on experimental design is available in the Nature Research Reporting Summary linked to this article.

Data availability. The data that support the findings of this study are available from the corresponding author upon reasonable request. No custom code was used in this study.

References

50. Rodríguez, C. I. et al. High-efficiency deleter mice show that FLPe is an alternative to Cre-loxP. *Nat. Genet.* **25**, 139–140 (2000).
51. Buffelli, M. et al. Genetic evidence that relative synaptic efficacy biases the outcome of synaptic competition. *Nature* **424**, 430–434 (2003).
52. Vong, L. et al. Leptin action on GABAergic neurons prevents obesity and reduces inhibitory tone to POMC neurons. *Neuron* **71**, 142–154 (2011).
53. Madisen, L. et al. Transgenic mice for intersectional targeting of neural sensors and effectors with high specificity and performance. *Neuron* **85**, 942–958 (2015).
54. Wichterle, H., Lieberam, I., Porter, J. A. & Jessell, T. M. Directed differentiation of embryonic stem cells into motor neurons. *Cell* **110**, 385–397 (2002).
55. Huberman, A. D. et al. Genetic identification of an On-Off direction-selective retinal ganglion cell subtype reveals a layer-specific subcortical map of posterior motion. *Neuron* **62**, 327–334 (2009).
56. Furuta, Y., Lagutin, O., Hogan, B. L. & Oliver, G. C. Retina- and ventral forebrain-specific Cre recombinase activity in transgenic mice. *Genesis* **26**, 130–132 (2000).
57. Suzuki, S. C. et al. Cadherin-8 is required for the first relay synapses to receive functional inputs from primary sensory afferents for cold sensation. *J. Neurosci.* **27**, 3466–3476 (2007).
58. Cai, D., Cohen, K. B., Luo, T., Lichtman, J. W. & Sanes, J. R. Improved tools for the Brainbow toolbox. *Nat. Methods* **10**, 540–547 (2013).
59. Buhusi, M. et al. ALCAM regulates mediolateral retinotopic mapping in the superior colliculus. *J. Neurosci.* **29**, 15630–15641 (2009).
60. Matsuda, T. & Cepko, C. L. Controlled expression of transgenes introduced by in vivo electroporation. *Proc. Natl Acad. Sci. USA* **104**, 1027–1032 (2007).
61. Dhande, O. S. & Crair, M. C. Transfection of mouse retinal ganglion cells by in vivo electroporation. *J. Vis. Exp.* **50**, 2678 (2011).
62. Trapnell, C. et al. Differential gene and transcript expression analysis of RNA-seq experiments with TopHat and Cufflinks. *Nat. Protoc.* **7**, 562–578 (2012).
63. Robinson, M. D., McCarthy, D. J. & Smyth, G. K. edgeR: a Bioconductor package for differential expression analysis of digital gene expression data. *Bioinformatics* **26**, 139–140 (2010).
64. Bolger, A. M., Lohse, M. & Usadel, B. Trimmomatic: a flexible trimmer for Illumina sequence data. *Bioinformatics* **30**, 2114–2120 (2014).
65. McLean, C. Y. et al. GREAT improves functional interpretation of cis-regulatory regions. *Nat. Biotechnol.* **28**, 495–501 (2010).
66. Picelli, S. et al. Full-length RNA-seq from single cells using Smart-seq2. *Nat. Protoc.* **9**, 171–181 (2014).
67. Adachi, H. et al. Stage-specific reference genes significant for quantitative PCR during mouse retinal development. *Genes Cells* **20**, 625–635 (2015).
68. Duan, X. et al. Subtype-specific regeneration of retinal ganglion cells following axotomy: effects of osteopontin and mTOR signaling. *Neuron* **85**, 1244–1256 (2015).
69. Choi, J. H. et al. Optimization of AAV expression cassettes to improve packaging capacity and transgene expression in neurons. *Mol. Brain* **7**, 17 (2014).
70. Euler, T. et al. Eyecup scope–optical recordings of light stimulus-evoked fluorescence signals in the retina. *Pflugers Arch.* **457**, 1393–1414 (2009).
71. Baden, T. et al. The functional diversity of retinal ganglion cells in the mouse. *Nature* **529**, 345–350 (2016).

nature research

Corresponding author(s): Joshua R Sanes

Life Sciences Reporting Summary

Nature Research wishes to improve the reproducibility of the work that we publish. This form is intended for publication with all accepted life science papers and provides structure for consistency and transparency in reporting. Every life science submission will use this form; some list items might not apply to an individual manuscript, but all fields must be completed for clarity.

For further information on the points included in this form, see Reporting Life Sciences Research. For further information on Nature Research policies, including our data availability policy, see Authors & Referees and the Editorial Policy Checklist.

Please do not complete any field with "not applicable" or n/a. Refer to the help text for what text to use if an item is not relevant to your study.
For final submission: please carefully check your responses for accuracy; you will not be able to make changes later.

Experimental design

1. Sample size

   Describe how sample size was determined.

   No statistical methods were used to pre-determine sample sizes but out sample sizes are similar to those reported in previous publications (Krishaswamy et al. 2015, Duan et al. 2014, Liu and Sanes 2017). At least 3 animals were analyzed per condition per genotype in each experiment and multiple independent measurements (cells) were taken from each animal. Exact numbers of animals and cells are provided in text and/or figure legends.

2. Data exclusions

   Describe any data exclusions.

   Exclusion criteria were pre-established for initial characterization of calcium responses in control animals (Supplementary Figure 6a-d) to eliminate noise due to technique. We counted only cells with quality index >0.45 and a z-score that was >1.0 for at least two consecutive time-points. For physiological comparisons across genotypes, all data were included. No other data were excluded.

3. Replication

   Describe the measures taken to verify the reproducibility of the experimental findings.

   All data was replicable, with the number of replicates (cells and animals) provided in text and/or figure legends.

4. Randomization

   Describe how samples/organisms/participants were allocated into experimental groups.

   Samples were allocated by genotype.

5. Blinding

   Describe whether the investigators were blinded to group allocation during data collection and/or analysis.

   No blinding was performed since phenotypes were assessed by definitive criteria that were applied consistently across all animals and cells.

Note: all in vivo studies must report how sample size was determined and whether blinding and randomization were used.

6. Statistical parameters

For all figures and tables that use statistical methods, confirm that the following items are present in relevant figure legends (or in the Methods section if additional space is needed).

n/a	Confirmed
☐	☒ The exact sample size (*n*) for each experimental group/condition, given as a discrete number and unit of measurement (animals, litters, cultures, etc.)
☐	☒ A description of how samples were collected, noting whether measurements were taken from distinct samples or whether the same sample was measured repeatedly
☐	☒ A statement indicating how many times each experiment was replicated
☐	☒ The statistical test(s) used and whether they are one- or two-sided *Only common tests should be described solely by name; describe more complex techniques in the Methods section.*
☐	☒ A description of any assumptions or corrections, such as an adjustment for multiple comparisons
☐	☒ Test values indicating whether an effect is present *Provide confidence intervals or give results of significance tests (e.g. P values) as exact values whenever appropriate and with effect sizes noted.*
☐	☒ A clear description of statistics including central tendency (e.g. median, mean) and variation (e.g. standard deviation, interquartile range)
☐	☒ Clearly defined error bars in all relevant figure captions (with explicit mention of central tendency and variation)

See the web collection on statistics for biologists for further resources and guidance.

Software

Policy information about availability of computer code

7. Software

Describe the software used to analyze the data in this study.

Generic functions on commercial or freely available software were used. They are as follows: ImageJ 1.49u, winDRP v1.6.4, Matlab R2015b, Imaris x64 7.4.0, Igor Pro 6.12A, R 3.1.3, Graphpad Prism 7.03.

For manuscripts utilizing custom algorithms or software that are central to the paper but not yet described in the published literature, software must be made available to editors and reviewers upon request. We strongly encourage code deposition in a community repository (e.g. GitHub). *Nature Methods* guidance for providing algorithms and software for publication provides further information on this topic.

Materials and reagents

Policy information about availability of materials

8. Materials availability

Indicate whether there are restrictions on availability of unique materials or if these materials are only available for distribution by a third party.

All unique materials are readily available from the authors or from standard commercial sources as stated in Methods.

9. Antibodies

Describe the antibodies used and how they were validated for use in the system under study (i.e. assay and species).

All antibodies, supplier name, catalog number, working dilutions are reported in Methods. Antibodies used were as follows: chicken anti-GFP (1:1000, Abcam ab13970), rabbit anti-Tbr1 (1:1000, Abcam ab31940, McKenna et al. 2011), rabbit anti-Tbr2 (1:500, Abcam ab23345), goat FoxP2 (1:1000, Abcam), guinea pig FoxP1 (1:5000, Ben Novitch), goat Satb1 (1:1000, Santa Cruz Biotechnology sc-5989X), goat Pcsk2 (1:1000, R&D Systems AF6018, Supplementary Figure 4e) rabbit anti-mCherry (1:5000, Cai et al. 2012), mouse anti-Cre (1:500, Millipore MAB3120), 1:1000, goat anti-VAchT (1:1000, Millipore ABN100), mouse anti-Brn3a (1:500, Millipore Mab1585), guinea pig anti-VAchT (1:500, Promega G4481), guinea pig Rbpms (1:500, PhosphoSolutions 1832-RBPMS), goat anti-Brn3b (1:500, Santa Cruz Biotechnology sc-6026), mouse anti-Brn3c (1:250, Santa Cruz Biotechnology sc-81980), rabbit anti-Calbindin (1:10000, Swant CB38a), rabbit anti-CART (1:2000, Phoenix Pharmaceuticals H-003-62), Syt2 (1:250, ZIRC Znp-1), goat anti-Opn (1:500, R&D Systems AF-808), goat Sorcs3 (1:1000, R&D systems AF3067, Figure 5d), mouse PKCa (1:500, Abcam ab31), goat anti-Alcam (1:1000, R&D systems AF1172, Buhusi et al. 2009), goat anti-Neo1 (1:1000, R&D systems AF1079, Supplementary Figure 8c) and rabbit β-galactosidase (1:5000 Duan et al. 2014). Dylight405-, Alexa488-, Cy3- and Alexa647-conjugated secondary antibodies (1:1000) were obtained from Jackson Immunoresearch. Unless stated otherwise, these antibodies have been previously validated in Rousso et al. 2016.

10. Eukaryotic cell lines

a. State the source of each eukaryotic cell line used.

No eukaryotic cell lines were used for results presented in this study.

b. Describe the method of cell line authentication used.

No eukaryotic cell lines were used in this study.

c. Report whether the cell lines were tested for mycoplasma contamination.

No eukaryotic cell lines were used in this study.

d. If any of the cell lines used are listed in the database of commonly misidentified cell lines maintained by ICLAC, provide a scientific rationale for their use.

No eukaryotic cell lines were used in this study.

Animals and human research participants

Policy information about studies involving animals; when reporting animal research, follow the ARRIVE guidelines

11. Description of research animals

Provide all relevant details on animals and/or animal-derived materials used in the study.

All mice used are reported in Methods. They are on a mixed CD1-C57BL6 background. No sex-specific differences were noted so animals were analyzed regardless of sex. Adult animals are defined as 21 days or older. Animals across developmental and adult stages were immunostained for expression analyses; all ages were reported in Results and Figure legends. Adults were used for calcium imaging. Electroporation and AAV injections were performed on postnatal day 0 pups; pups are sacrificed at P12-14. P5-6 mice were used for J-RGC RNAseq.

Policy information about studies involving human research participants

12. Description of human research participants

Describe the covariate-relevant population characteristics of the human research participants.

The study did not involve human research participants.